Adaptive optics ophthalmoscopy: application to age-related macular degeneration and vascular diseases

Michel Paques, Serge Meimon, Florence Rossant, David Rosenbaum, Sarah Mrejen, Florian Sennlaub, Kate Grieve

Adaptive optics ophthalmoscopy: application to age-related macular degeneration and vascular diseases

Michel Paques[1], Serge Meimon[2], Florence Rossant[3], David Rosenbaum[4], Sarah Mrejen[1], Florian Sennlaub[5], Kate Grieve[1]

[1]Centre Hospitalier National d'Ophtalmologie des Quinze-Vingts, INSERM-DHOS Clinical Investigation Center 1423, Paris, France.

[2]ONERA - The French Aerospace Lab, 92320 Châtillon, France

[3]Institut Supérieur d'Electronique de Paris, 75006 Paris, France

[4]Unité de prévention cardiovasculaire, Salpêtrière Hospital, UPMC Univ Paris 06

[5]Institut de la Vision, 17 rue Moreau, Sorbonne Universités, UPMC Univ Paris 06, INSERM, CNRS, 75012 Paris, France.

†Correspondence should be addressed to: Prof Michel Paques, Paris Adaptive Optics Retinal Imaging and Surgery (PARIS) group; Tel: (33) 1 40 02 14 15 Fax: (33) 1 53 46 26 93; Email: mp@cicoph.org

Adaptive optics ophthalmoscopy: application to age-related macular degeneration and vascular diseases

Abstract

Adaptive optics (AO)-enhanced *en face* retinal imaging, termed here AO ophthalmoscopy (AOO) has reached a level of robustness which fosters its expanding use in research and clinical centers. Here we will review the contribution of clinical AOO to the understanding and monitoring of 1) age-related macular degeneration and 2) vascular diseases. The main contributions of AOO to the phenotyping of AMD are a better identification of drusen, a better delineation of the limits of atrophy, and the identification of novel features such as punctate hyperreflectivity and mobile melanin clumps. Characterization of progression of atrophy is facilitated by time-lapse AOO. In vessels AOO imaging enables the observation and measurement of parietal structures and the observation of microscopic pathological features such as small hemorrhages and inflammatory cell accumulations.

19 # Contents

42

43

1. Introduction

The first observation of the fundus of the eye in the nineteenth century led to the foundation of modern ophthalmology. Until recently, however, the retina itself could not be directly observed because it is translucent and hence faintly visible by fundus photography. It was the advent of techniques allowing a higher contrast such as optical coherence tomography (OCT) in the 1990s and then adaptive optics (AO)-enhanced ophthalmoscopy (AOO) in the 2000s that made neuroretinal structures directly observable in vivo. The first demonstration of the clinical interest of AOO was reported in 1997 in Liang, Miller and William's seminal work using an AO fundus camera[1] which allowed observation of cone photoreceptors. Since then, by achieving diffraction-limited resolution in clinically usable, robust systems, visualization of previously unseen structures such as individual photoreceptors and vessel walls can now be done in a routine fashion. Thanks to the convergence of technical maturity and better understanding of the contribution of AOO imaging, its use in research and clinical centers is expanding worldwide, in ophthalmology and beyond. Several reviews of AOO have been done previously[2-5]. In the present review, we will focus on the contribution of AOO to the understanding of age-related macular degeneration (AMD) and vascular diseases, and suggest some perspectives for improvement in these areas. We will limit this review to en face fundus camera and scanning AOO systems, excluding adaptive optics optical coherence tomography (AO-OCT) which has not yet been applied to the same extent to AMD and vasculature in patients. Readers interested in AO-OCT may refer to several reviews[6,7].

2. AO ophthalmoscopy (AOO) technologies

High resolution imaging of the retina faces several challenges, including optical aberrations arising from the anterior segment and the limited reflectance of the retina. These challenges are tackled by AO which counteracts optical aberrations in real-time with a

deformable mirror, whose shape is derived from wavefront measurements via a real-time control loop, in order to increase light throughput and resolution. AOO has been performed with flood illumination fundus cameras, scanning laser ophthalmoscopes (SLO) and OCT[6,7]. Fundus camera systems use flood illumination to capture a two dimensional en face image in a single shot using a two dimensional camera as detector. SLO systems scan point by point (or line by line) in a raster fashion over the retina and collect the backscattered light with a single-pixel detector. Fundus camera and scanning AOO systems yield different results (**Fig. 1**). Fundus camera images show inherently less motion-induced distortion than scanning systems, which is of interest in the case of poor fixation, at the cost of reduced contrast. The main advantage of SLO systems is the use confocal detection to reject light from out of focus layers and so achieve high axial resolution and contrast. SLO systems have also benefitted from alternative detection schemes (known as split detection, offset aperture or dark field) that capture multiply scattered photons that do not pass through the confocal pinhole. Eliminating the strongest signal, which tends to emanate from directionally dependent waveguided light from photoreceptor outer segments and the highly scattering nerve fibers and vessels, enables detection of more weakly reflective structures, for example photoreceptor inner segments[8], retinal pigment epithelium (RPE)[9,10] and retinal ganglion cells[11].

In the text that follows, for scanning AOO images we will call the directly backscattered light that passes through the confocal pinhole the "bright field" mode, and the multiply scattered light which is offset from the confocal pinhole the "dark field" mode. The ability to separate the different sources of contrast in these different modalities can provide clues as to the origin of the features we observe and hence their clinical signification.

3. Dry age-related macular degeneration

AMD is a leading cause of blindness in developed countries[12,13]. Despite the identification of several genetic, molecular and environmental factors[14,15], the pathophysiology of AMD

remains debated and in its dry form there is currently no available treatment. Histopathological changes of dry AMD affect the outer retina, the RPE and the inner choroid[16]. The dominant paradigm states that AMD results from cumulative damage affecting the interaction between the photoreceptors and the RPE cells related to genetically determined low grade subretinal inflammation[17]. Over decades, cumulative low level damage challenges the resilience of the outer retina; the sight-threatening complications of AMD are therefore the clinical manifestation of a rupture and/or exhaustion of chronically activated compensatory mechanisms.

Clinically, an early/intermediate phase moderately affecting vision is followed by a late stage at which sight-threatening complications are observed. Funduscopically, the canonical lesions of early/intermediate AMD are drusen and/or pseudodrusen, basal linear deposits (which are focal thickening of the Bruch's membrane) and pigmentary changes. Transition from early to late dry AMD occurs when spots of Bruch's membrane devoid of RPE are detected. The disruption of the RPE monolayer (grographic atrophy) is indeed the key event leading to blindness, because it is temporally and spatially linked to loss of cones and to the advent of an absolute scotoma[18]. Here, we will describe the most notable contributions of AOO to the phenotyping of AMD, and compare the knowledge about histology and pathophysiology of dry AMD to AOO. Most of the histology data presented here is from the Project Macula developed by Christine Curcio and the University of Alabama of Birmingham (www. *projectmacula.cis.uab.edu*)[19].

3.1. Early stage AMD

Drusen are composed of focal deposits of extracellular debris in contact with the RPE. Drusen are hallmarks of AMD. Each druse subtype bears a specific risk of evolution to late stages of AMD. Three main drusen phenotypes have been characterized: either under the RPE ("conventional" soft drusen, and cuticular drusen) or over the RPE (subretinal drusenoid

119 deposits (SDD, also called reticular pseudodrusen). Spaide, Curcio and co-authors have
120 hypothesized that their different imaging and histologic characteristics are due to differences
121 in location and biogenesis[20-23].

122 Figure 2 illustrates the fundus camera AOO appearance of the different types of drusen by
123 comparison with non-AO corrected near infrared (nIR) SLO images. Conventional drusen
124 appear on AOO as subtle variations in the grayscale tones, with a variably hyperreflective
125 center. Drusen are usually surrounded by a continuous or discontinuous hyporeflectivity and
126 sometimes an incomplete dark ring. Some conventional drusen appeared more reflective than
127 others, with a better contrast from the background areas[24,25]. Cone photoreceptors are detected
128 overlying conventional drusen and the cone density has been found to be moderately reduced
129 over conventional drusen. The differences in reflectivity of conventional drusen may be due
130 to differences in sub-RPE material reflectivity as these variations can be seen on SD-OCT as
131 well, and also to variable degrees of depigmentation and thinning of the overlying RPE. These
132 hypotheses need to be further investigated through mutlimodal imaging integrating nIR
133 autofluorescence to evaluate the degrees of RPE degeneration associated with conventional
134 drusen. Some authors showed that RPE atrophy predates the collapse of large conventional
135 drusen by analysing the sequence of events in OCT over time.[26,27]

136 Cuticular drusen correspond to the innumerable mosaic of small and uniformly sized
137 drusen visualized on fluorescein angiography (FA) and indocyanine green (ICG) angiography.
138 With AOO their reflectivity profile is variable; they may appear as a hyporeflective center
139 with a hyperreflective rim or diffusely hyperreflective. Different patterns of reflectivity could
140 be found in the same eye, as has also been described with nIR scanning laser ophthalmoscopy
141 (SLO)[28]. These different reflectivity aspects found within the same eye could correspond
142 either to different evolutive stages or to different types of cuticular drusen, but also to the
143 degree of depigmentation and thinning of the overlying RPE.

144 SDD have a specific reflectivity in AOO, with a hyperreflective core of variable size
145 circled by a dark rim of constant width; this aspect has been confirmed on both fundus camera
146 and scanning AOO systems. In addition, numerous dark dots can be visualized around the
147 areas of larger SDD that were not visualized around conventional drusen with AOO or other
148 imaging modalities; these may correspond to smaller stage 1 or 2 SDD not discriminated with
149 conventional nIR SLO imaging. Meadway et al analyzed the microstructure of stage 3 SDD
150 using scanning AOO and AO OCT and showed that the speckled appearance over SDD of
151 grossly similar shape and reflectivity as photoreceptors was rather due to the granules of the
152 lesion material itself[29]. AOO helped demonstrate that SDD were composed of material that
153 accumulates in the same tissue compartment as photoreceptors above the RPE and associated
154 with major perturbations of photoreceptors. Zhang et al also demonstrated the dynamism of
155 SDD with scanning AOO over 12 months, analyzing 269 solitary SDD in 6 eyes of 4
156 patients[30]. They showed that there were new and regressed SDD lesions over time and that the
157 percentage of sampled retinal areas affected by these ranged from 0.7% to 9.3%.
158 A peculiar situation is small drusen of young subjects. On bright field scanning AOO
159 images, these drusen appear as round, oval or lobular areas of diameter 22-61 µm where cone
160 photoreceptor reflectivity and density are decreased[31] usually associated with discrete
161 thickening of the RPE complex. The outline and size of these lesions corresponds to 1-4 RPE
162 cells, hence giving rise to the hypothesis that small, hard drusen could arise from very few
163 RPE cells. When high in density, these may represent the earliest stage of druse; yet the extent
164 to which these findings apply to age-related drusen remains to be determined.

165 ## 3.2 Late AMD ("geographic atrophy")

166 ### 3.2.1 Atrophy margins

167 **Figure 3** shows an example of montage of fundus camera AOO images of a dry AMD
168 case. **Figure 4** compares the different modalities of AOO imaging. The margins of atrophic

169 areas show a variety of aspects, ranging from well-defined to ill-defined (**Figure 5**). With
170 fundus camera AOO, well-defined margins are often hyporeflective, further enhancing their
171 contrast and also suggesting that they contain melanin clumps; it is however possible that
172 retinal disorganization also contributes to the hyporeflectivity of the margins. Ill-defined
173 atrophy margins on the other hand are very difficult to delineate unambiguously. In these
174 cases, tracing a limit between the preserved RPE monolayer and the atrophic area is highly
175 subjective, particularly if there are overlapping foci of hyporeflective clumps (HRCs). These
176 HRCs are indeed more numerous in ill-defined than in well-defined borders. During the
177 follow-up of AMD patients, comparing successive AOO images can demonstrate progression
178 of atrophic lesions within a relatively short time frame (**Fig. 6**)[32].

179 The persistence of an "island' of intact RPE monolayer under the fovea in the midst of an
180 area of RPE atrophy, called foveal sparing, is often observed. Despite the preservation of
181 central visual acuity, the resulting tunnel-like vision is often a severe handicap. Conceivably,
182 in these cases even a small progression of RPE atrophy towards the fovea will be associated
183 with severe visual loss. While short wavelength autofluorescence imaging is impaired by the
184 presence of the xanthophyll pigment which blurs the limits of preserved RPE[33,34], AOO
185 enables an exquisite delineation of such areas[32,35] (**Fig. 4**).

186 ### 3.2.2 Cone mosaic and punctate hyperreflectivity

187 In preserved areas of dry AMD eyes, the cone mosaic is often dim in AOO images, with a
188 high spatial variability of reflectivity; such poor visibility of the cone mosaic is further
189 accentuated at the edge of GA lesions[36]. It remains uncertain if the altered visibility is due to
190 the actual loss of cones or to the alteration of their optical properties. Histology shows that
191 cones at lesion margins have altered morphology[16,37, 38] which may contribute to their poor
192 visibility. This poor visibility of the cone mosaic is in striking contrast with the observation of
193 a bright hyperreflective granular structure within atrophic regions mimicking the normal cone

194 photoreceptor mosaic. This is consistently observed on different cases, with both fundus
195 camera and scanning AOO (**Fig. 7**) although the bright field mode of scanning AOO yields
196 the highest contrast for this specific feature. The density of such punctate hyperreflectivity
197 (PHR) is within the range of the normal cone density (unpublished data). Since PHR
198 resembles the cone mosaic, it may correspond to photoreceptor remnants. Histology studies of
199 AMD indeed showed that in atrophic areas there may be remnants of cone inner segments[39].
200 However, these inner segments remnants are sparse, irregularly dispersed and lack outer
201 segments which make them unlikely to have such a bright hyperreflectance and regular
202 disposition.

203 Basal laminar deposits (BlamD) are sub-RPE deposits that are a hallmark of the aging
204 Bruch's membrane[40]. They are made of a continuous material deposition between the RPE
205 basal membrane and Bruch's membrane. When devoid of RPE cells, the BlamD may persist
206 and form a continuous layer which is spiky on its inner surface and smooth on its outer
207 surface[41, 42] (i.e. in contact with Bruch's membrane) (**Fig. 8**). Hence, reflectance over the
208 BlamD may theoretically generate a mosaic-like reflectance similar to the PHR. In order to
209 better understand the origin of PHR, directional imaging may be helpful since the Stiles-
210 Crawford effect may facilitate the identification of cone photoreceptors[43,44]. If the BlamD is
211 indeed involved, then the similarity of the PHR and cone mosaic raises the question of the
212 possible interference of the reflectance from both structures (i.e., the cone mosaic and BlamD)
213 in non-atrophic areas. This may contribute to the abovementioned poor visibility of the cone
214 mosaic.

215 3.2.3. Hyporeflective clumps (HRCs)

216 Fundoscopic examination and histology shows that extensive melanin redistribution
217 accompanies all stages of AMD[37,45]. In histology this is seen in the earliest steps of AMD in
218 the form of rearrangement of intracellular melanosomes, leading to an uneven distribution of

219 melanin. During late AMD, more marked changes can be observed, the most remarkable
220 being the presence of hyporeflective clumps (HRCs) dispersed over the RPE monolayer as
221 well as within atrophic areas. These HRCs have been attributed to detached RPE cells[37]
222 and/or to a non-RPE cell type (possibly microglia[46,47] or monocyte-macrophages that have
223 phagocytized RPE cells[48]). Many HRCs indeed show cytological characteristics very close to
224 those of RPE cells; at the same time, the unequivocal presence of subretinal and sub-RPE
225 macrophages identified using immunohistological markers such as CD163, IBA-1 and
226 CCR2[48,49] have been reported in eyes with dry AMD. A significant number of subretinal
227 macrophages indeed contain melanosomes, presumably from ingested RPE cells. It is possible
228 that HRCs in the outer nuclear layer account for the hyperflective foci seen with OCT during
229 AMD[46]. A histological taxonomy of human HRCs based on their shape and location has been
230 recently proposed[19]. This classification distinguishes bilaminar, sloughed, dissociated,
231 shedding, and entombed types.

232 A consistent feature of AO fundus camera images of dry AMD is the presence of a myriad
233 of HRCs dispersed over the posterior pole (**Fig. 5 and 9**). Although the size of HRCs varies
234 greatly, they typically appear as black dots measuring around 20µm[32] , hence similar to the
235 size of melanin containing cells seen in histology. As histology suggests that melanosomes
236 remain mostly intracellular even at late stages of the disease, HRCs can be considered as
237 intracellular tags for most of them. HRCs can be detected over the atrophic areas as well as
238 over the RPE monolayer (albeit with a lower contrast in the latter case). It is surprising to note
239 that HRCs are of low contrast in scanning AOO; HRCs are indeed much better detected by
240 fundus camera AOO than by scanning AOO (**Fig. 9**).

241 HRCs appear to colocalize with hyper-nIR autofluorescence (nIRAF)[32,50], although the
242 colocalization of HRCs and hyper-nIRAF can at present only be hypothesized based on
243 comparison of images of unequal resolution. Use of an nIRAF-capable AOO system such as

244 that used in (Granger, Williams, Rossi, ARVO E-abstract 3429, 2017) could provide an
245 answer to this question.
246 When comparing successive AOO fundus images of dry AMD taken over a period of
247 several months, extensive changes in the distribution of HRCs are consistently observed.
248 When adequate time sampling is done (i.e. at a rate of approximately one image per month),
249 time-lapse sequences unequivocally demonstrate that there is motion of many HRCs[32].
250 Migration of HRCs is the most dynamic process that has been identified to date in AMD; it
251 can indeed be detected over a timescale of days while atrophy progression is only detectable
252 over a timescale of weeks. One may hypothesize that such activity represents a reactive
253 process following degeneration. In this regard, it is of interest to note that migration of HRCs
254 is also observed over non atrophic areas (i.e. over the intact RPE monolayer). This indicates
255 that such cell motility may be present early in the course of AMD, and hence is not solely an
256 effect of cone photoreceptor degeneration. The velocity of HRCs is highly heterogeneous, and
257 can reach a magnitude of one micrometer a day. They show a complex migration that defies
258 classification. Most show limited, erratic motion, while some seem to progress in parallel to
259 atrophy progression. Very few show a directional progression (**Fig. 10 and 11**). The
260 significance of such motion is uncertain; displacement of HRCs may not necessarily imply
261 that an entire cell is moving. Indeed, intracellular motion of melanosomes may account for
262 <10μm scale motion of HRCs. To our knowledge there is very limited documentation of cell
263 migration in the living retina. It has been showed that microglial and infiltrating macrophage
264 cells can migrate in response to damage to the RPE[47].
265 Although it is a speculative approach, some correspondence between this taxonomy and
266 AOO imaging of HRCs may be postulated (**Fig. 12**). Along progression fronts, cells in the
267 pigmented borders are probably of the "bilaminar" phenotype, i.e. with a layer of HRCs over
268 the RPE monolayer. Highly contrasted HRCs dispersed over the RPE monolayer outside of

margins are possibly HRCs of the “sloughed” type. Similar HRCs over RPE atrophy may be cells of the “dissociated” type. The migration pattern of HRCs may also contribute to classify them into this taxonomy. Migration is probably facilitated in the subretinal space; it may therefore be assumed that HRCs of the “sloughed” phenotype are more likely to show migration. On the other hand, “subducted” HRCs (i.e. located between the BlamD and the Bruch’s membrane) are probably less mobile because they are embedded in remodeled tissues. Very small static melanin spots may be “shed RPE cells”, i.e. whose melanosomes are embedded into subretinal material.

3.2.4 Outer retinal tubulations

Within atrophic areas there are frequently tubular, 50-100µm wide arborescent structures , termed outer retinal tubulations (ORT)[51]. ORTs contain radially oriented cones and Müller cell extensions[52-54]. The presence of ORTs shows that cones may survive for a relatively long duration in atrophic areas. Fundus camera and scanning AOO can both detect the outlines of ORTs (**figure 13**)[55]. It has been shown that scanning AOO can detect cone structure within ORTs[56]. It has been postulated that this configuration is a survival strategy for cones[49] albeit their potential for functional recovery is unknown. The possibility of detecting (and hence monitoring) surviving cones within ORTs may be of interest to characterize the resilience of cones in dystrophic retinas, and may also guide RPE grafting since an area with cone persistence may be most appropriate.

3.3 Perspectives for AOO of dry AMD

The complex features of dry AMD are progressively being unveiled using a variety of imaging techniques, among which AOO will probably play a major role. Investigating the correspondence of AOO images with histology will be crucial to improve the rationale for their interpretation.

293 Current cell culture technology can achieve a functionally and phenotypically normal RPE
294 mosaic[57], and even sub-RPE deposits mimicking drusen[58]. Hence, it can be expected that
295 imaging RPE cell cultures may be an acceptable surrogate for *in vivo* imaging of RPE aging
296 and diseases.
297 A higher short-wavelength autofluorescence signal along lesional margins is predictive of
298 progression[59]. En face imaging of tissue samples offers some useful support for image
299 interpretation, showing for instance the colocalization of lipofuscin and melanin at a
300 microscopic level (**Figure 14**).[60,61] One can hence speculate that accumulation of HRCs along
301 the margins of atrophy may be linked to the increased short wavelength autofluorescence.
302 Hence, the link between short-wavelength autofluorescence and AMD progression is possibly
303 explained by the presence of HRCs at the margins of atrophy. Accordingly, a recent clinical
304 study suggested that pigmentary changes are predictive of progression.[62]
305 Analyzing the migration of HRCs is still a challenge. It is known that HRCs may migrate
306 into the inner retina[19] and hence escape the focus plane of AOO. Therefore, migrating patterns
307 of HRCs may be more accurately defined by taking into consideration their depth disposition
308 within the retinal layers as well. Time-lapse volumetric OCT may therefore contribute to a
309 better tracking of HRCs within the depth of the retina, while AOO may be most suitable for
310 those migrating close to the RPE.
311 In vivo observation of the RPE cells is still far from being a routine procedure, although it
312 has recently shown interesting perspectives using AO-enhanced indocyanine green
313 angiography[63], AO-enhanced short wavelength[10] and infrared autofluorescence[64] and two-
314 photon imaging[65]. Given that technical robustness and absence of light toxicity is
315 demonstrated, this may be of interest to analyze the fate of individual RPE cells, which would
316 help to clarify the origin of HRCs. The choriocapillaris is still difficult to analyze in detail in
317 vivo although AO-OCT[66] has recently shown interesting perspectives. Finally, wet AMD is

still difficult to explore with AOO because of the combination of loss of retinal transparency and the complex 3D arrangement of lesions.

4. Vascular imaging

The retina relies on a finely tuned blood flow for its supply of metabolites and metabolic signals and for disposal of waste products. The planar disposition of retinal vessels make them conveniently observable with *en face* imaging. The exponential relationship between lumen diameter and conductance (Poiseuille's law) highlights the importance of high precision measurement of vascular diameters. The retinal vessels are cognates of brain vessels, sharing many functional and pathological features; hence, retinal vessels may be considered in many aspects as surrogates of brain vessels. Age, hypertension and diabetes are the most common factors influencing the morphology and function of microvessels. With the advent of AOO, not only did measurement of lumen diameter with micrometric precision become possible, but also structural imaging[67]. Dedicated software for automated segmentation of arteries has been developed which facilitates the extraction of clinically relevant biomarkers.[68]

4. 1 Normal vessels

AOO imaging of vessels shows the red blood cell column as a dark line with a specular reflex along its crest. Along arteries and sometimes along veins, the walls can be seen as thin, laminated bands (**Fig. 15**). With fundus camera AOO, there is also a hyperreflective halo surrounding the vessels, possibly due to the backscattering of laterally reflected incident light. It is thought that the inner limit of the wall corresponds to the plasma-endothelial interface, and that the outer limit represents the outer limit of the adventicia. Within the wall of arteries a central hyporeflective band can be identified (**Fig. 16**) which possibly corresponds to the media containing smooth muscle cells[67]. This central hyporeflective band is more apparent over lightly pigmented RPE (not shown), highlighting the role of backscattered light in its

visualization. AOO can also detect discrete structures (**Fig. 16, right**), presumably comprising pericytes.

AOO offered for the first time the possibility to measure directly the thickness of the wall and hence to calculate the wall-to-lumen ratio (WLR) in vivo[69]. Assuming a correct anatomical correspondence, the median WLR of normal arterioles is ~0.28; WLR increases when the size of the artery decreases[70]. The WLR of normal veins is around 0.1; no lamination has been yet observed in the venous wall.

At arterial bifurcations, the specular reflex along the vessel crest is divided along daughter branches, while at venous confluences each specular reflex can be followed after the confluence (**Fig**. **17**).[71] This demonstrates that red blood cells, which remain in distinct columns after venous confluences, contribute to the axial specular reflex.

The geometry of the arteriolar arborescence is an essential determinant of its energetic efficiency[72]. Based on the minimal work principle, Murray's laws state that for achieving the conflictual requirements of minimization of shear stress and blood volume, blood flow should be proportional to the cube of the vessel radii[73]. Because of the conservation of flow, this implies that at arterial bifurcations there is a cubic relationship between the radii of parent (P) and daughter vessels (D_1 and D_2). Hence in a symmetrical bifurcation there is a homothetical factor (i.e. a relative variation of diameter of downstream vessels) of 0.79. These laws, established on theoretical grounds, were verified in vivo only in the 1970s[74]. The junction coefficient (X solving $P^x=D_1^x + D_2^x$, for which the expected value is 3) is a convenient way of quantifying the conformation of a microvascular network to Murray's laws. **Figure 18** illustrates the changes in X consecutive to changes in vessel diameters in an optimal bifurcation. This shows that an increased X means a better conductance of flow downward to the bifurcation, either because of an increased daughter (D) or a decreased parent (P). Hence, at a particular bifurcation, deviation of X from 3 parallels flow conductance.

In retinal vessels, deviation from optimality has been associated with peripheral arterial diseases[75], incident heart disease, stroke[76] and diabetes[77], yet these conclusions were drawn from conventional fundus photographs; hence blur may have altered the precision of the measurements. Using AOO, in normal arteries a median value of X of 2.8 in arteries and of 2.3 in veins has been reported[78], both being significantly inferior to 3. The cause of this physiological deviation from Murray's laws remains to be determined.

Retinal capillaries have a complex, multilayered 3D arrangement. A serial arrangement of these layers has been documented in rodents[79,80] and pigs[81], yet remains to be confirmed in the primate retina. Fine details of capillaries are visible with bright field scanning AOO but are only faintly detectable with AOO fundus cameras[82]. Offset imaging with motion contrast has proven effective to image capillaries.[83,84] Indeed, differential analysis between two images specifically detects fast moving particles, that is, red blood cells. Viewing of retinal capillaries using oral fluorescein angiography has also been demonstrated[85]. **Figure 19** shows an example of a montage of scanning AOO images of capillaries. AOO is not yet capable of imaging wide field volumes to cover the whole complex 3D retinal capillary network. Nevertheless, capillary imaging and flow measurements in the perifoveal ring have a clear clinical interest because of the disproportional importance of the fovea for vision relative to its size. The flow of leukocytes in individual capillaries and the flow in the perifeoveal capillaries has been reported[86,87] in which velocities between 0 and 1.2mm/sec were measured. By using a combination of scanning AOO and computational fluid dynamics analysis, it has been shown that wall shear stress can be estimated in vivo in human perifoveal capillaries[88].

4. 2 Vascular aging and hypertension

The most common manifestations of aging/hypertensive retinopathy are diffusely increased WLR and focal lesions such as focal arteriolar narrowings (FANs) and

392 arteriovenous nickings (AVNs). These features have been the subject of a considerable
393 amount of research as predictive biomarkers of end-organ damage[89]. Several large scale
394 epidemiological studies reported that the severity and/or incidence of these signs correlate
395 with end-organ damage[90]. Hypertensive microvasculopathy is also suspected to play a role in
396 Alzheimer's disease[91]. It is of importance to note that atherosclerosis (atheroma), i.e. the
397 presence in the subintima of cholesterol plaques, affects only large arteries and hence does not
398 affect retinal vessels.

399 ### 4.2.1 Parietal thickening

400 The WLR of arterioles is a fundamental indicator of the effect of arterial hypertension on
401 small vessels. Increased WLR occurs through the chronic stimulation by blood pressure of the
402 myogenic reflex (Bayliss effect)[92], a process leading to eutrophic remodelling. Fundus
403 photograph-based studies reported an age and pressure-related decline of the lumen diameter
404 of arteries, which may be interpreted as indirect evidence of parietal thickening[93]. However,
405 despite some interesting results using differential Doppler and reflectance imaging[92], until the
406 advent of AOO, there was no convenient clinical method to measure the WLR. Since then,
407 several teams have shown that the WLR measured with AOO correlates well with blood
408 pressure[69,95-98]. Ageing also decreases the diameter of the lumen and the parietal thickness,
409 hence increasing the WLR. The effect of blood pressure on the WLR is therefore age-
410 dependant, with a stronger correlation in young subjects[95].

411 Measurement of the WLR in the retina appears to be an interesting tool for management of
412 arterial hypertension. Since change in the WLR occurs in a matter of weeks, it is rather
413 immune to acute changes in blood pressure; hence, it is possible that the WLR is an integrator
414 of past blood pressure. Considering the WLR may thus help to overcome the problem of
415 stress-induced variation of blood pressure (so-called "white coat hypertension"). After a few
416 weeks of antihypertensive treatment introduction, a significant increase in internal diameter

417 was reported[95] leading to a decreased WLR. Interestingly, this was observed irrespective of
418 the pharmacological class, suggesting that the effect of antihypertensive drugs on small
419 vessels is mediated by blood pressure, rather than through a direct pharmacological effect on
420 small vessels. AOO has been used to detect short-term changes in vascular morphometry
421 following surgical treatment of resistant hypertension[99].

422 4.2.2 Focal vascular lesions: arteriovenous nickings and focal 423 arteriolar narrowing

424 While most scientific research and hence conceptual efforts in hypertensive
425 microvasculopathy are addressed to diffuse changes of parietal thickness, little attention is
426 paid to focal microvascular changes. This is partly due to the fact that these changes are
427 difficult to capture with histology. Moreover, their natural history is poorly documented.
428 Narrowing and deformation of veins in the vicinity of arteries defines AVNs. The latter are
429 surrogates of cerebrovascular aging and are also the direct cause of retinal vein occlusions.
430 There has been a longstanding yet unsubstantiated consensus among clinicians about the
431 compressive nature of the arteriovenous conflict underlying AVNs. This belief persists
432 despite the fact that histology studies failed to evidence arteriovenous compression; instead,
433 histology consistently pointed to extravascular changes identified as glial proliferation, glial
434 edema[100] or extracellular deposits[101], as the cause of AVNs.
435 Using AOO we have shown that the WLR does not differ between AVNs and normal
436 arteriovenous crossings, ruling out parietal thickening as the cause of AVNs[69]. However, to
437 analyze the interface between an artery and a vein at an arteriovenous crossing, optical access
438 to the interface is necessary, which is usually not possible using reflectance imaging because
439 the interposition of the artery. This can be overcome by analyzing a specific yet uncommon
440 vascular pattern, that is, cases in which focal venous remodeling is observed where an artery
441 and a vein are close yet not overlapping ; these cases can reasonably be considered as "non-

442 crossing" AVNs[102]. Indeed, veins adjacent to arterioles may undergo marked phenotypical
443 changes identical to AVNs (i.e. nicking, narrowing, opacification and/or dragging) without
444 any physical arteriovenous contact as demonstrated by AOO (**Fig. 20**). These findings support
445 and extend the conclusions of histology stating that the paradigm of arterial crushing as the
446 cause of venous nicking stems from a misinterpretation of fundus photographs.

447 During aging, irregularities in the caliber of arteries are also commonly observed. The
448 most obvious manifestation is the presence of FANs, i.e. a clinically detectable focal
449 reduction of arteriolar caliber. Given the exponential relationship between lumen diameter
450 and flow conductance, even a limited, focal reduction in diameter may have significant
451 hemodynamic consequences. Theoretically, FANs may be due to parietal thickening or focal
452 vasoconstriction. In all cases of FANs that we examined, the outer limit of the wall remained
453 parallel to the internal wall (**Fig. 20, top)**, that is, there was no evidence of local parietal
454 thickening. Moreover, we frequently observed disappearance of FANs (**Fig. 20, bottom**),
455 which strongly argues for chronic vasoconstriction being the cause of FANs. The presence of
456 FANs may thus be an indicator of a dysregulation of the microvascular tone.

457 ## 4. 3 Diabetic retinopathy

458 Diabetic retinopathy (DR) is a leading cause of visual loss in working-age adults
459 worldwide[103-105]. Histology shows that loss of pericytes and endothelial cells occur early in
460 DR, being detectable in experimental diabetes long before there is any macroscopic sign of
461 DR. DR is hence considered as resulting from the cumulative effect of progressive loss of
462 canonical functions of retinal capillaries leading to a combination of nonperfusion and
463 hyperpermeability. The very first clinically detectable changes seen in vivo are
464 microaneurysms surrounded by capillary occlusions.

465 AOO is promising for the detection of early capillary changes. At the earliest stages of DR
466 (i.e. in the absence of clinically gradable diabetic retinopathy), capillary dilation[106],

467 tortuosity[83, 107] and disruption of capillaries[108] have been reported. A higher flow velocity than
468 controls has also been reported.[109] Recently, alteration of the junction coefficient has been
469 confirmed by an AOO study in diabetics[78].

470 The internal structure of microaneurysms has been explored with scanning AOO using a
471 combination of reflectance and fluorescence angiography[107]. This study showed that
472 microaneurysms have a variably thickened wall. At more advanced stages of DR, an
473 exquisitely fine documentation of microscopic features such as microaneurysms,
474 microhemorrages, and hard exudates (**Fig.21**) can also be obtained with AOO.

475 4. 4 Vascular inflammation

476 Because vessels are physiologically in contact with innate and adaptive immune effectors,
477 they are at the crossroads of a variety of inflammatory diseases. Accordingly, retinal vascular
478 inflammation is a common feature during various types of uveitis, which can be detected on
479 fundus images under the form of perivascular sheathing and/or focal disruption of the blood-
480 retinal barrier. Veins are more often affected than arteries by inflammation. Post-capillary
481 venules are the elective site of extravasation of blood-borne inflammatory cells (diapedesis).
482 Given the diagnostic and prognostic value of perivascular sheathing, it would be of clinical
483 interest to better identify, quantify and monitor retinal vasculitis. Thanks to the high
484 sensitivity of AO to loss of retinal transparency, paravascular cellular infiltrates constitutive
485 of retinal vasculitis can be detected with high precision (**Fig. 22**).[110] Perivascular
486 inflammation can be located on one or both sides of vessels, over a width of several tens of
487 micrometers, up to several millimeters along the affected vessel. Focal reduction of venous
488 diameter often accompanies perivascular sheathing. In the example showed in **figure 23**,
489 perivascular sheathing was accompanied by local deformation of the adjacent NFL,
490 suggesting that in this particular case venous narrowing may have been due to compression
491 from the infiltrate.

4. 5 Perspectives for AOO in vascular imaging

Because microvascular structure, motricity and flow can be analyzed with AOO with high precision, a better knowledge of the pathophysiology of human microvasculature will undoubtedly emerge from future clinical studies and technological development based on AOO. Fine morphometric measurements are a promising approach because they may enable identification of subtle changes of perfusion homeostasis at an early stage.

The complex spatial and functional organization of retinal capillaries makes comprehensive mapping of retinal microvessels challenging with AAO; on the other hand, a better understanding of this organization will enable the design of specific procedures. For instance, the deep vascular layer is electively affected by capillary remodelling in DR[111] and retinal vein occlusions[80,112]. Postcapillary venules, which are located for the most part in this same layer are also the preferential site of leukocyte adherence and diapedesis. Hence, targeting the deep microvessel layer may offer more precise insights into several processes affecting microvessels. Similarly, targeting the perifoveal capillaries may be relevant for diseases affecting the macula.

The oxygen saturation of red cells can be measured in the retina using differential light absorption[113]. Current techniques for oxymetry, however, are limited to medium to large vessels; in the future, AOO-enhanced oxymetry techniques may provide access to oxygen saturation of capillaries. Measuring the biomechanics of the systolic pulse on retinal vessels offers an interesting approach for evaluating the stiffness of large vessels. It is possible to document microvasculature caliber and tortuosity changes during the cardiac cycle with scanning AOO[67] and fundus camera AOO[114]. Such mechanotransmission has been the subject of extensive studies in the cardiovascular field[115] since it is believed that the velocity of the systolic pulse is related to parietal stiffness.

516 The natural history of early stages microvascular aging, of DR and of hypertensive
517 retinopathy remains poorly documented with AOO. At the earliest stages of DR, AOO study
518 of capillary flow may help to solve controversies about retinal blood flow changes[116,117].
519 Functional studies at the capillary level (neurovascular coupling[118]) may also be of interest, as
520 a decreased efficiency of neurovascular coupling in the retina is present early in diabetes[119].
521 Longitudinal AOO studies may contribute to a better knowledge of the natural history of the
522 development of microaneurysms, capillary nonperfusion and exudates. In particular,
523 documenting the loss of pericytes[71] offers also interesting perspectives.

524 ## 5. AOO in clinical trials

525 Clinical trials in ophthalmology increasingly rely on imaging. More precise biomarkers
526 allow earlier results with fewer patients, and are therefore ethically necessary. However, while
527 the use of OCT in clinical trials has been developing at an exponential pace, AO-enhanced
528 imaging has lagged behind. The current technological level of robustness and the possibility
529 to obtain quantitative biomarkers already permits the integration of AO in large scale trials in
530 AMD, arterial hypertension and vasculitis. For trials in AMD, emergence and progression of
531 small atrophic spots are the most straightforward applications. A particular interest of AOO is
532 to enable precise monitoring of the residual RPE in cases of foveal sparing. Cell therapy using
533 RPE cell grafts has been proposed to treat atrophic AMD[120]; time-lapse AOO would be of
534 interest to follow the fate of grafted cells. In arterial hypertension, WLR is a robust,
535 dimensionless parameter that can be measured on large cohorts of nondilated patients. Several
536 epidemiological studies on retinal vessel imaging using AO, including pediatric cohorts, are
537 underway. A promising perspective of AOO is the follow-up of patients treated by
538 antihypertensive drugs. The retina indeed offers the unique possibility to measure the effect of
539 vasoactive drugs. It would be of interest to determine if early 'microvascular responders' (i.e.,
540 those patients showing vasodilation under therapy) have a better prognosis in terms of

541 reduction of end-organ damage. In inflammatory diseases, the size of inflammatory infiltrates
542 around vessels may also be considered as a biomarker of interest. The contribution of AOO to
543 trials in diabetic retinopathy is promising. For instance, AOO may better document the
544 turnover of microaneurysms; another application would be the measurement of the
545 morphometry of arterial bifurcations.

546 ## 6. Conclusions

547 Most medical specialists can only dream of the highly precise imaging that we
548 ophthalmologists can routinely achieve using AOO. AOO may force us to rethink the
549 physiopathological concepts of many diseases affecting the retina. As Sydney Brenner said,
550 "progress in science depends on new techniques, new discoveries and new ideas, probably in
551 that order". By enabling quantitative in vivo "optical biopsy", high resolution imaging may
552 find many medical applications in a spectrum of indications, spanning from ophthalmology to
553 general medicine. The possibility to perform a fine quantitative analysis is of obvious interest
554 for monitoring diseases. Diseases that show slow progression at a macroscopic scale can
555 reveal significantly more activity at a smaller scale. The applications of AOO to other public
556 health diseases such as arterial hypertension and diabetes will bring support from the
557 pharmaceutical industry which may further boost clinical developments of AOO.

558 AOO is a rapidly changing field and the range of its medical applications is constantly
559 increasing[1]; the reader should therefore keep in mind that our review is at risk of rapid
560 obsolescence. For instance, while long considered unfeasible, visualization of human retinal
561 ganglion cells[11] was recently demonstrated. There are still several hurdles that hinder the full
562 integration of AOO in routine clinics and trials. Several factors such as technical complexity,
563 cost, interpretative schemes and integration of AOO images into management of patients still
564 need to be improved. These topics are the subject of a multidisciplinary effort of physicists,
565 computer scientists, ophthalmologists, and histologists. Improving knowledge of histology

566 and of light-tissue interactions will be useful. Investigation of light-tissue interactions using
567 similar techniques in vitro and in vivo[121] will help to improve the rationale of image
568 interpretation. Among other questions is the fact that structures may have a different aspect in
569 scanning and fundus camera AOO. Acquiring more clinical experience, using accurate
570 metrics and building large normative databases will improve image interpretation. Image
571 processing and analysis software should be customized to diseases and biomarkers and
572 combine multimodal information. Then, more adequate training schemes, standard
573 procedures, and biomarkers for trials may be developed. Trials in healthcare domains other
574 than ophthalmology will be facilitated with the use of user-friendly, automated, nonmydriatic
575 instruments.

576 ## Acknowledgements

577 Jonathan Benesty, Celine Chaumette, Marie-Hélène Errera, Elena Gofas-Salas, Céline
578 Faure, Xavier Girerd, Edouard Koch, Chahira Miloudi, Pedro Mecê, Hasan Sawan, José-Alain
579 Sahel, Valérie Sarda, Andrea Sodi, Iyed Trimèche and the patients that participated in our
580 studies.

581 This work was supported by the Institut National de la Santé et de la Recherche Médicale
582 (Contrat d'Interface 2011), the Agence Nationale de la Recherche (ANR-12-TECS-0015-03,
583 LabEx LIFESENSES ANR-10-LABX-65, ANR-11-IDEX-0004-02), the Foundation Fighting
584 Blindess (C-CL-0912-0600-INSERM01, C-GE-0912-0601-INSERM02), the Thome
585 Foundation and the European Research Council (ERC-SyG 610110). The funding
586 organization had no role in the design or conduct of this research. Original data provided here
587 are from a clinical research study (ClinicalTrials.gov NCT0154618).

References

1. Liang, J., Williams, D. R. & Miller, D. T. Supernormal vision and high-resolution retinal imaging through adaptive optics. *J. Opt. Soc. Am. A Opt. Image Sci. Vis.* **14,** 2884–2892 (1997).

2. Roorda A. Applications of adaptive optics scanning laser ophthalmoscopy. Optom Vis Sci. 2010 Apr; 87(4):260-8.

3. Godara P, Dubis AM, Roorda A, Duncan JL, Carroll J. Adaptive Optics Retinal Imaging: Emerging Clinical Applications. Optom Vis Sci. 2010;87(12):930-941.

4. Roorda, A. & Duncan, J. L. Adaptive optics ophthalmoscopy. *Annu. Rev. Vis. Sci.* **1,** 19–50 (2015)

5. Marcos, S. *et al.* Vision science and adaptive optics, the state of the field. *Vision Res.* **132,** 3–33 (2017).

6. Jonnal R. S. *et al.* A Review of Adaptive Optics Optical Coherence Tomography: Technical Advances, Scientific Applications, and the Future. *Invest. Ophthalmol. Vis. Sci.* **57,** 51-68

7. Pircher M, Zawadzki RJ. Review of adaptive optics OCT (AO-OCT): principles and applications for retinal imaging [Invited]. Biomed Opt Express. 2017 Apr 19;8(5):2536-2562

8. Scoles, D. *et al.* In vivo imaging of human cone photoreceptor inner segments. *Invest. Ophthalmol. Vis. Sci.* **55,** 4244–4251 (2014).

9. Scoles, D., Sulai, Y. N. & Dubra, A. In vivo dark-field imaging of the retinal pigment epithelium cell mosaic. *Biomed. Opt. Express* **4,** 1710–1723 (2013).

10. Rossi, E. A. *et al.* In vivo imaging of retinal pigment epithelium cells in age related macular degeneration. *Biomed. Opt. Express* **4,** 2527–2539 (2013).

11. Rossi, E. A. *et al.* Imaging individual neurons in the retinal ganglion cell layer of the living eye. *Proc. Natl. Acad. Sci. U. S. A.* **114,** 586–591 (2017).

613 12. Robman, L. D. *et al.* Age-related macular degeneration in ethnically diverse Australia:
614 Melbourne Collaborative Cohort Study. *Ophthalmic Epidemiol.* **22,** 75–84 (2015).
615 13. Klein, R. *et al.* Prevalence of age-related macular degeneration in the US population.
616 *Arch. Ophthalmol. Chic. Ill 1960* **129,** 75–80 (2011).
617 14. Ardeljan, D. & Chan, C.-C. Aging is not a disease: distinguishing age-related macular
618 degeneration from aging. *Prog. Retin. Eye Res.* **37,** 68–89 (2013).
619 15. Ambati, J. & Fowler, B. J. Mechanisms of age-related macular degeneration. *Neuron*
620 **75,** 26–39 (2012)
621 16. Bird, A. C., Phillips, R. L. & Hageman, G. S. Geographic atrophy: a histopathological
622 assessment. *JAMA Ophthalmol.* 132, 338–345 (2014).
623 17. Guillonneau X, Eandi CM, Paques M, Sahel JA, Sapieha P, Sennlaub F. On phagocytes
624 and macular degeneration. Prog Ret Eye Res 2017;61: 98-128.
625 18. Panorgias, A. *et al.* Multimodal assessment of microscopic morphology and retinal
626 function in patients with geographic atrophy. *Invest. Ophthalmol. Vis. Sci.* **54,** 4372–4384
627 (2013).
628 19. Zanzottera, E. C. *et al.* The Project MACULA Retinal Pigment Epithelium Grading
629 System for Histology and Optical Coherence Tomography in Age-Related Macular
630 Degeneration. *Invest. Ophthalmol. Vis. Sci.* **56,** 3253–3268 (2015).
631 20. Spaide RF, Curcio CA. Drusen characterization with multimodal imaging. Retina.
632 2010;30:1441-1454.
633 21. Curcio CA, Messinger JD, Sloan KR, et al. Subretinal drusenoid deposits in non-
634 neovascular age-related macular degeneration: morphology, prevalence, topography, and
635 biogenesis model. Retina. 2013;33:265-276
636 22. Spaide RF, Curcio CA, Zweifel SA. Drusen, an old but new frontier. Retina.
637 2010;30:1163-1165.

638 23. Zweifel SA, Spaide RF, Curcio CA, et al. Reticular pseudodrusen are subretinal
639 drusenoid deposits. Ophthalmology. 2010;117:303-312 e301
640 24. Mrejen, S., Sato, T., Curcio, C. A. & Spaide, R. F. Assessing the cone photoreceptor
641 mosaic in eyes with pseudodrusen and soft Drusen in vivo using adaptive optics
642 imaging. *Ophthalmology* **121,** 545–551 (2014).
643 25. Querques, G. *et al.* Appearance of medium-large drusen and reticular pseudodrusen on
644 adaptive optics in age-related macular degeneration. *Br. J. Ophthalmol.* **98,** 1522–1527
645 (2014).
646 26. Balaratnasingam C, Messinger JD, Sloan KR, et al. Histologic and Optical Coherence
647 Tomographic Correlates in Drusenoid Pigment Epithelium Detachment in Age-Related
648 Macular Degeneration. Ophthalmology. 2017;124:644-656.
649 27. Balaratnasingam C, Yannuzzi LA, Curcio CA, et al. Associations Between Retinal
650 Pigment Epithelium and Drusen Volume Changes During the Lifecycle of Large
651 Drusenoid Pigment Epithelial Detachments. Invest Ophthalmol Vis Sci. 2016;57:5479-
652 5489
653 28. Balaratnasingam C, Cherepanoff S, Dolz-Marco R, et al. Cuticular Drusen: Clinical
654 Phenotypes and Natural History Defined Using Multimodal Imaging. Ophthalmology.
655 2018;125:100-118.
656 29. Meadway, A., Wang, X., Curcio, C. A. & Zhang, Y. Microstructure of subretinal
657 drusenoid deposits revealed by adaptive optics imaging. *Biomed. Opt. Express* **5,** 713–
658 727 (2014)
659 30. Zhang, Y. *et al.* DYNAMISM OF DOT SUBRETINAL DRUSENOID DEPOSITS IN
660 AGE-RELATED MACULAR DEGENERATION DEMONSTRATED WITH
661 ADAPTIVE OPTICS IMAGING. *Retina Phila. Pa* **38,** 29–38 (2018)

662 31. Pedersen, H. R. *et al.* Multimodal imaging of small hard retinal drusen in young healthy
663 adults. *Br. J. Ophthalmol.* **102,** 146–152 (2018).
664 32. Gocho, K. *et al.* Adaptive optics imaging of geographic atrophy. *Invest. Ophthalmol.*
665 *Vis. Sci.* **54,** 3673–3680 (2013).
666 33. Schmitz-Valckenberg, S. *et al.* In vivo imaging of foveal sparing in geographic atrophy
667 secondary to age-related macular degeneration. *Invest. Ophthalmol. Vis. Sci.* **50,** 3915–
668 3921 (2009).
669 34. Lindner, M. *et al.* Directional Kinetics of Geographic Atrophy Progression in Age-
670 Related Macular Degeneration with Foveal Sparing. *Ophthalmology* **122,** 1356–1365
671 (2015).
672 35. Querques, G. *et al.* ADAPTIVE OPTICS IMAGING OF FOVEAL SPARING IN
673 GEOGRAPHIC ATROPHY SECONDARY TO AGE-RELATED MACULAR
674 DEGENERATION. *Retina Phila. Pa* **36,** 247–254 (2016). ^
675 36. Zayit-Soudry, S., Duncan, J. L., Syed, R., Menghini, M. & Roorda, A. J. Cone structure
676 imaged with adaptive optics scanning laser ophthalmoscopy in eyes with nonneovascular
677 age-related macular degeneration. *Invest. Ophthalmol. Vis. Sci.* **54,** 7498–7509 (2013)
678 37. Zanzottera, E. C. *et al.* VISUALIZING RETINAL PIGMENT EPITHELIUM
679 PHENOTYPES IN THE TRANSITION TO GEOGRAPHIC ATROPHY IN AGE-
680 RELATED MACULAR DEGENERATION. *Retina Phila. Pa* **36 Suppl 1,** S12–S25
681 (2016).
682 38. Eandi CM, Messance HC, Augustin S, Dominguez E, Lavalette S, Forster V, Hu SJ,
683 Siquieros L, Craft CM, Sahel JA, Tadayoni R, Paques M, Guillonneau X, Sennlaub F.
684 Subretinal mononuclear phagocytes induce cone segment loss via IL-1β. eLife 2016;5:e16490
685 39. Curcio, C. A., Medeiros, N. E. & Millican, C. L. Photoreceptor loss in age-
686 relatedmacular degeneration. *Invest. Ophthalmol. Vis. Sci.* **37,** 1236–1249 (1996).

687 40. Sarks, S., Cherepanoff, S., Killingsworth, M. & Sarks, J. Relationship of Basal Laminar
688 Deposit and Membranous Debris to the Clinical Presentation of Early Age-Related
689 Macular Degeneration. *Invest. Ophthalmol. Vis. Sci.* **48,** 968–977 (2007).
690 41. Tan ACS, Astroz P, Dansingani KK, Slakter JS, Yannuzzi LA, Curcio CA, Bailey
691 Freund K. The Evolution of the Plateau, an Optical Coherence Tomography Signature
692 Seen in Geographic Atrophy. *Invest. Ophthalmol. Vis. Sci.* 2017;58:2349-2358.
693 42. Ooto S, Vongkulsiri S, Sato T, Suzuki M, Curcio CA, Spaide RF. Outer Retinal
694 Corrugations in Age-Related Macular Degeneration. JAMA Ophthalmol.
695 2014;132(7):806-813.
696 43. Panorgias, A. *et al.* Multimodal assessment of microscopic morphology and retinal
697 function in patients with geographic atrophy. *Invest. Ophthalmol. Vis. Sci.* **54,** 4372–4384
698 (2013).
699 44. Miloudi, C. *et al.* The Negative Cone Mosaic: A New Manifestation of the Optical
700 Stiles-Crawford Effect in Normal Eyes. *Invest. Ophthalmol. Vis. Sci.* **56,** 7043–7050
701 (2015).
702 45. Zanzottera, E. C., Messinger, J. D., Ach, T., Smith, R. T. & Curcio, C. A. Subducted and
703 melanotic cells in advanced age-related macular degeneration are derived from retinal
704 pigment epithelium. *Invest. Ophthalmol. Vis. Sci.* **56,** 3269–3278 (2015).
705 46. Curcio, C. A., Zanzottera, E. C., Ach, T., Balaratnasingam, C. & Freund, K. B.
706 Activated Retinal Pigment Epithelium, an Optical Coherence Tomography Biomarker
707 for Progression in Age-Related Macular Degeneration. *Invest. Ophthalmol. Vis. Sci.* **58,**
708 BIO211-BIO226 (2017).
709 47. Paques, M. *et al.* In vivo observation of the locomotion of microglial cells in the retina.
710 *Glia* **58,** 1663–1668 (2010).

711 48. Sennlaub, F. *et al.* CCR2(+) monocytes infiltrate atrophic lesions in age-related macular
712 disease and mediate photoreceptor degeneration in experimental subretinal inflammation in
713 Cx3cr1 deficient mice. *EMBO Mol. Med.* **5,** 1775–1793 (2013).
714 49. Combadière, C. *et al.* CX3CR1-dependent subretinal microglia cell accumulation is
715 associated with cardinal features of age-related macular degeneration. *J. Clin. Invest.* **117,**
716 2920–2928 (2007).
717 50. Kellner, U., Kellner, S. & Weinitz, S. Fundus autofluorescence (488 NM) and near-
718 infrared autofluorescence (787 NM) visualize different retinal pigment epithelium alterations
719 in patients with age-related macular degeneration. *Retina Phila. Pa* **30,** 6–15 (2010).
720 51. Zweifel, S. A. *et al.* Outer retinal tubulation: a novel optical coherence tomography
721 finding. *Arch. Ophthalmol. Chic. Ill 1960* **127,** 1596–1602 (2009).
722 52. Litts, K. M. *et al.* Clinicopathological correlation of outer retinal tubulation in age-
723 related macular degeneration. *JAMA Ophthalmol.* **133,** 609–612 (2015).
724 53. Litts, K. M., Messinger, J. D., Freund, K. B., Zhang, Y. & Curcio, C. A. Inner Segment
725 Remodeling and Mitochondrial Translocation in Cone Photoreceptors in Age-Related
726 Macular Degeneration With Outer Retinal Tubulation. *Invest. Ophthalmol. Vis. Sci.* **56,** 2243–
727 2253 (2015).
728 54. Litts, K. M. *et al.* Quantitative Analysis of Outer Retinal Tubulation in Age-Related
729 Macular Degeneration From Spectral-Domain Optical Coherence Tomography and Histology.
730 *Invest. Ophthalmol. Vis. Sci.* **57,** 2647–2656 (2016).
731 55. Litts, K. M. *et al.* EXPLORING PHOTORECEPTOR REFLECTIVITY THROUGH
732 MULTIMODAL IMAGING OF OUTER RETINAL TUBULATION IN ADVANCED AGE-
733 RELATED MACULAR DEGENERATION. *Retina Phila. Pa* **37,** 978–988 (2017).
734 56. King, B. J. *et al.* SD-OCT and Adaptive Optics Imaging of Outer Retinal Tubulation.
735 *Optom. Vis. Sci. Off. Publ. Am. Acad. Optom.* **94,** 411–422 (2017).

736 57. Reichman, S. *et al.* Generation of Storable Retinal Organoids and Retinal Pigmented
737 Epithelium from Adherent Human iPS Cells in Xeno-Free and Feeder-Free Conditions. *Stem*
738 *Cells Dayt. Ohio* **35,** 1176–1188 (2017).
739 58. Pilgrim, M. G. *et al.* Subretinal Pigment Epithelial Deposition of Drusen Components
740 Including Hydroxyapatite in a Primary Cell Culture Model. *Invest. Ophthalmol. Vis. Sci.* **58,**
741 708–719 (2017)
742 59. Holz, F. G. *et al.* Progression of geographic atrophy and impact of fundus
743 autofluorescence patterns in age-related macular degeneration. *Am. J. Ophthalmol.* **143,** 463–
744 472 (2007).
745 60. Pollreisz, A. *et al.* Visualizing melanosomes, lipofuscin, and melanolipofuscin in human
746 retinal pigment epithelium using serial block face scanning electron microscopy. *Exp. Eye*
747 *Res.* **166,** 131–139 (2017).
748 61. Holz, F. G., Steinberg, J. S., Göbel, A., Fleckenstein, M. & Schmitz-Valckenberg, S.
749 Fundus autofluorescence imaging in dry AMD: 2014 Jules Gonin lecture of the Retina
750 Research Foundation. *Graefes Arch. Clin. Exp. Ophthalmol. Albrecht Von Graefes Arch. Klin.*
751 *Exp. Ophthalmol.* **253,** 7–16 (2015).
752 62. Ferrara, D. *et al.* Optical Coherence Tomography Features Preceding the Onset of
753 Advanced Age-Related Macular Degeneration. *Invest. Ophthalmol. Vis. Sci.* **58,** 3519–3529
754 (2017).
755 63. Tam, J., Liu, J., Dubra, A. & Fariss, R. In Vivo Imaging of the Human Retinal Pigment
756 Epithelial Mosaic Using Adaptive Optics Enhanced Indocyanine Green Ophthalmoscopy.
757 *Invest. Ophthalmol. Vis. Sci.* **57,** 4376–4384 (2016).
758 64. Morgan, J. I. W., Dubra, A., Wolfe, R., Merigan, W. H. & Williams, D. R. In Vivo
759 Autofluorescence Imaging of the Human and Macaque Retinal Pigment Epithelial Cell
760 Mosaic. *Invest. Ophthalmol. Vis. Sci.* **50,** 1350–1359 (2009).

761 65. Sharma, R., Williams, D. R., Palczewska, G., Palczewski, K. & Hunter, J. J. Two-
762 Photon Autofluorescence Imaging Reveals Cellular Structures Throughout the Retina of the
763 Living Primate Eye. *Invest. Ophthalmol. Vis. Sci.* **57,** 632–646 (2016).
764 66. Kurokawa, K., Liu, Z. & Miller, D. T. Adaptive optics optical coherence tomography
765 angiography for morphometric analysis of choriocapillaris [Invited]. *Biomed. Opt. Express* **8,**
766 1803 (2017).
767 67. Chui, T. Y. P., Gast, T. J. & Burns, S. A. Imaging of vascular wall fine structure in the
768 human retina using adaptive optics scanning laser ophthalmoscopy. *Invest. Ophthalmol. Vis.*
769 *Sci.* **54,** 7115–7124 (2013).
770 68. Lermé, N. *et al.* A fully automatic method for segmenting retinal artery walls in adaptive
771 optics images. *Pattern Recognit. Lett.* **72,** 72–81 (2016).
772 69. Koch, E. *et al.* Morphometric analysis of small arteries in the human retina using
773 adaptive optics imaging: relationship with blood pressure and focal vascular changes. *J.*
774 *Hypertens.* **32,** 890–898 (2014).
775 70. Meixner, E. & Michelson, G. Measurement of retinal wall-to-lumen ratio by adaptive
776 optics retinal camera: a clinical research. *Graefes Arch. Clin. Exp. Ophthalmol. Albrecht Von*
777 *Graefes Arch. Klin. Exp. Ophthalmol.* **253,** 1985–1995 (2015).
778 71. Chui, T. Y. P., Vannasdale, D. A. & Burns, S. A. The use of forward scatter to improve
779 retinal vascular imaging with an adaptive optics scanning laser ophthalmoscope. *Biomed. Opt.*
780 *Express* **3,** 2537–2549 (2012).
781 72. Murray, C. D. The Physiological Principle of Minimum Work: I. The Vascular System
782 and the Cost of Blood Volume. *Proc. Natl. Acad. Sci. U. S. A.* **12,** 207–214 (1926).
783 73. Mayrovitz, H. N. & Roy, J. Microvascular blood flow: evidence indicating a cubic
784 dependence on arteriolar diameter. *Am. J. Physiol.* **245,** H1031-1038 (1983).

785 74. Zamir, M., Medeiros, J. A. & Cunningham, T. K. Arterial bifurcations in the human
786 retina. *J. Gen. Physiol.* **74,** 537–548 (1979).
787 75. Chapman, N. *et al.* Peripheral vascular disease is associated with abnormal arteriolar
788 diameter relationships at bifurcations in the human retina. *Clin. Sci. Lond. Engl. 1979* **103,**
789 111–116 (2002).
790 76. Witt, N. W. *et al.* A novel measure to characterise optimality of diameter relationships at
791 retinal vascular bifurcations. *Artery Res.* **4,** 75–80 (2010).
792 77. Sasongko, M. B. *et al.* Alterations in retinal microvascular geometry in young type 1
793 diabetes. *Diabetes Care* **33,** 1331–1336 (2010).
794 78. Luo, T., Gast, T. J., Vermeer, T. J. & Burns, S. A. Retinal Vascular Branching in
795 Healthy and Diabetic Subjects. *Invest. Ophthalmol. Vis. Sci.* **58,** 2685–2694 (2017).
796 79. Paques, M. *et al.* Structural and hemodynamic analysis of the mouse retinal
797 microcirculation. *Invest. Ophthalmol. Vis. Sci.* **44,** 4960–4967 (2003).
798 80. Genevois, O. *et al.* Microvascular remodeling after occlusion-recanalization of a branch
799 retinal vein in rats. *Invest. Ophthalmol. Vis. Sci.* **45,** 594–600 (2004).
800 81. Fouquet, S., Vacca, O., Sennlaub, F. & Paques, M. The 3D Retinal Capillary Circulation
801 in Pigs Reveals a Predominant Serial Organization. *Invest. Ophthalmol. Vis. Sci.* **58,** 5754–
802 5763 (2017).
803 82. Lombardo, M. *et al.* Analysis of retinal capillaries in patients with type 1 diabetes and
804 nonproliferative diabetic retinopathy using adaptive optics imaging. *Retina Phila. Pa* **33,**
805 1630–1639 (2013).
806 83. Tam, J., Martin, J. A. & Roorda, A. Noninvasive visualization and analysis of parafoveal
807 capillaries in humans. *Invest. Ophthalmol. Vis. Sci.* **51,** 1691–1698 (2010).

808 84. Sulai, Y. N., Scoles, D., Harvey, Z. & Dubra, A. Visualization of retinal vascular
809 structure and perfusion with a nonconfocal adaptive optics scanning light ophthalmoscope. *J.*
810 *Opt. Soc. Am. A Opt. Image Sci. Vis.* **31,** 569–579 (2014).
811 85. Pinhas, A. *et al.* In vivo imaging of human retinal microvasculature using adaptive
812 optics scanning light ophthalmoscope fluorescein angiography. *Biomed. Opt. Express* **4,**
813 1305–1317 (2013).
814 86. Martin, J. A. & Roorda, A. Direct and noninvasive assessment of parafoveal capillary
815 leukocyte velocity. *Ophthalmology* **112,** 2219–2224 (2005).
816 87. Arichika, S., Uji, A., Ooto, S., Miyamoto, K. & Yoshimura, N. Adaptive optics-assisted
817 identification of preferential erythrocyte aggregate pathways in the human retinal
818 microvasculature. *PloS One* **9,** e89679 (2014).
819 88. Lu, Y. *et al.* Computational fluid dynamics assisted characterization of parafoveal
820 hemodynamics in normal and diabetic eyes using adaptive optics scanning laser
821 ophthalmoscopy. *Biomed. Opt. Express* **7,** 4958–4973 (2016).
822 89. Hanff, T. C. *et al.* Retinal microvascular abnormalities predict progression of brain
823 microvascular disease: an atherosclerosis risk in communities magnetic resonance imaging
824 study. *Stroke* **45,** 1012–1017 (2014).
825 90. Yatsuya, H. *et al.* Retinal microvascular abnormalities and risk of lacunar stroke:
826 Atherosclerosis Risk in Communities Study. *Stroke* **41,** 1349–1355 (2010).
827 91. Cheung, C. Y.-L., Ong, Y.-T., Ikram, M. K., Chen, C. & Wong, T. Y. Retinal
828 microvasculature in Alzheimer's disease. *J. Alzheimers Dis. JAD* **42 Suppl 4,** S339-352
829 (2014).
830 92. Heagerty, A. M., Aalkjaer, C., Bund, S. J., Korsgaard, N. & Mulvany, M. J. Small artery
831 structure in hypertension. Dual processes of remodeling and growth. *Hypertens. Dallas Tex*
832 *1979* **21,** 391–397 (1993).

833 93. Kawasaki, R. *et al.* Retinal vessel diameters and risk of hypertension: the Multiethnic
834 Study of Atherosclerosis. *J. Hypertens.* **27,** 2386–2393 (2009).
835 94. Harazny, J. M. *et al.* New software analyses increase the reliability of measurements of
836 retinal arterioles morphology by scanning laser Doppler flowmetry in humans. *J. Hypertens.*
837 **29,** 777–782 (2011).
838 95. Rosenbaum, D. *et al.* Effects of age, blood pressure and antihypertensive treatments on
839 retinal arterioles remodeling assessed by adaptive optics. *J. Hypertens.* **34,** 1115–1122 (2016).
840 96. Rosenbaum, D. *et al.* Relationships between retinal arteriole anatomy and aortic
841 geometry and function and peripheral resistance in hypertensives. *Hypertens. Res. Off. J. Jpn.*
842 *Soc. Hypertens.* **39,** 536–542 (2016).
843 97. Hillard, J. G., Gast, T. J., Chui, T. Y. P., Sapir, D. & Burns, S. A. Retinal Arterioles in
844 Hypo-, Normo-, and Hypertensive Subjects Measured Using Adaptive Optics. *Transl. Vis.*
845 *Sci. Technol.* **5,** (2016).
846 98. Arichika, S., Uji, A., Ooto, S., Muraoka, Y. & Yoshimura, N. Effects of age and blood
847 pressure on the retinal arterial wall, analyzed using adaptive optics scanning laser
848 ophthalmoscopy. *Sci. Rep.* **5,** 12283 (2015).
849 99. Gallo, A., Rosenbaum, D., Kanagasabapathy, C. & Girerd, X. Effects of carotid
850 baroreceptor stimulation on retinal arteriole remodeling evaluated with adaptive optics camera
851 in resistant hypertensive patients. *Ann. Cardiol. Angeiol. (Paris)* **66,** 165–170 (2017).
852 100. Kimura, T., Mizota, A., Fujimoto, N. & Tsuyama, Y. Light and electron microscopic
853 studies on human retinal blood vessels of patients with sclerosis and hypertension. *Int.*
854 *Ophthalmol.* **26,** 151–158 (2005).
855 101. Jefferies, P., Clemett, R. & Day, T. An anatomical study of retinal arteriovenous
856 crossings and their role in the pathogenesis of retinal branch vein occlusions. *Aust. N. Z. J.*
857 *Ophthalmol.* **21,** 213–217 (1993).

858 102. Paques, M. *et al.* Venous Nicking Without Arteriovenous Contact: The Role of the
859 Arteriolar Microenvironment in Arteriovenous Nickings. *JAMA Ophthalmol.* **133,** 947–950
860 (2015).
861 103. Raman, R., Gella, L., Srinivasan, S. & Sharma, T. Diabetic retinopathy: An epidemic at
862 home and around the world. *Indian J. Ophthalmol.* **64,** 69–75 (2016).
863 104. Grauslund, J., Green, A. & Sjølie, A. K. Blindness in a 25-year follow-up of a
864 population-based cohort of Danish type 1 diabetic patients. *Ophthalmology* **116,** 2170–2174
865 (2009).
866 105. Cheung, N., Mitchell, P. & Wong, T. Y. Diabetic retinopathy. *Lancet Lond. Engl.* **376,**
867 124–136 (2010).
868 106. Burns, S. A. *et al.* In vivo adaptive optics microvascular imaging in diabetic patients
869 without clinically severe diabetic retinopathy. *Biomed. Opt. Express* **5,** 961–974 (2014)
870 107. Dubow, M. *et al.* Classification of human retinal microaneurysms using adaptive optics
871 scanning light ophthalmoscope fluorescein angiography. *Invest. Ophthalmol. Vis. Sci.* **55,**
872 1299–1309 (2014).
873 108. Tam, J. *et al.* Disruption of the retinal parafoveal capillary network in type 2 diabetes
874 before the onset of diabetic retinopathy. *Invest. Ophthalmol. Vis. Sci.* **52,** 9257–9266
875 (2011).
876 109. Arichika, S. *et al.* Retinal hemorheologic characterization of early-stage diabetic
877 retinopathy using adaptive optics scanning laser ophthalmoscopy. *Invest. Ophthalmol. Vis.*
878 *Sci.* **55,** 8513–8522 (2014).
879 110. Errera, M.-H. *et al.* Retinal vasculitis imaging by adaptive optics. *Ophthalmology* **121,**
880 1311–1312.e2 (2014).

881 111. Couturier, A. *et al.* CAPILLARY PLEXUS ANOMALIES IN DIABETIC
882 RETINOPATHY ON OPTICAL COHERENCE TOMOGRAPHY ANGIOGRAPHY. *Retina*
883 *Phila. Pa* **35,** 2384–2391 (2015).
884 112. Suzuki, N. *et al.* Microvascular Abnormalities on Optical Coherence Tomography
885 Angiography in Macular Edema Associated With Branch Retinal Vein Occlusion. *Am. J.*
886 *Ophthalmol.* **161,** 126–132.e1 (2016).
887 113. Linsenmeier, R. A. & Zhang, H. F. Retinal oxygen: from animals to humans. *Prog.*
888 *Retin. Eye Res.* **58,** 115–151 (2017).
889 114. Duan, A., Bedggood, P. A., Metha, A. B. & Bui, B. V. Reactivity in the human retinal
890 microvasculature measured during acute gas breathing provocations. *Sci. Rep.* **7,** (2017).
891 115. Vlachopoulos, C. *et al.* The role of vascular biomarkers for primary and secondary
892 prevention. A position paper from the European Society of Cardiology Working Group on
893 peripheral circulation: Endorsed by the Association for Research into Arterial Structure and
894 Physiology (ARTERY) Society. *Atherosclerosis* **241,** 507–532 (2015).
895 116. Burgansky-Eliash, Z. *et al.* Reduced retinal blood flow velocity in diabetic retinopathy.
896 *Retina Phila. Pa* **30,** 765–773 (2010).
897 117. Burgansky-Eliash, Z. *et al.* Increased retinal blood flow velocity in patients with early
898 diabetes mellitus. *Retina Phila. Pa* **32,** 112–119 (2012).
899 118. Newman, E. A. Functional hyperemia and mechanisms of neurovascular coupling in
900 the retinal vasculature. *J. Cereb. Blood Flow Metab. Off. J. Int. Soc. Cereb. Blood Flow*
901 *Metab.* **33,** 1685–1695 (2013).
902 119. Lecleire-Collet, A. *et al.* Evaluation of retinal function and flicker light-induced retinal
903 vascular response in normotensive patients with diabetes without retinopathy. *Invest.*
904 *Ophthalmol. Vis. Sci.* **52,** 2861–2867 (2011).

905 120. Schwartz, S. D., Tan, G., Hosseini, H. & Nagiel, A. Subretinal Transplantation of
906 Embryonic Stem Cell-Derived Retinal Pigment Epithelium for the Treatment of Macular
907 Degeneration: An Assessment at 4 Years. *Invest. Ophthalmol. Vis. Sci.* **57,** ORSFc1-9 (2016).
908 121. Grieve, K., Thouvenin, O., Sengupta, A., Borderie, V. M. & Paques, M. Appearance of
909 the Retina With Full-Field Optical Coherence Tomography. *Invest. Ophthalmol. Vis. Sci.* **57,**
910 OCT96-OCT104 (2016).
911
912
913
914

Figure legends

Figure 1: Comparison of fundus camera (left column) vs bright field scan (right column) AOO, showing normal photoreceptors (top row), an artery (center row), and an atrophy zone during dry age-related macular degeneration.

Figure 2. Imaging of drusen. Top row, near infrared scanning laser ophthalmoscopy (nIR SLO) imaging; center row, OCT; bottom row, fundus camera AOO. (A, D, G) Conventional drusen appear as subtle variations in the grayscale tones surrounded by discontinuous hyporeflectivity on the fundus camera AOO. (B, E, H) cuticular drusen distributed in a continuous pattern are clearly distinguished on corresponding AOO. (C, F, I) subretinal drusenoid deposits (SDD) are visible by AOO as hyperreflective cores of variable sizes surrounded by dark annulus of constant width. Some of the dark dots (arrows) may correspond to smaller stage 1 or 2 SDD.

Figure 3: Montage of fundus camera AOO images of a case of dry AMD.

Figure 4. Case of foveal sparing seen by SLO, OCT, fundus camera AOO and scanning AOO in bright and dark field modes.

Figure 5. Example of ill-defined (top) and well-defined (bottom) lesions viewed with fundus camera AOO.

Figure 6: Illustration of progression of GA. (A) SLO infrared image. (B, C) two AOO fundus camera images taken 1 month apart. The horizontal lines and the arrow in (C) facilitate the identification of the progression of atrophy. Note also the rearrangement of HRCs outside of the atrophic area (compare the pattern of pigment distribution in the circles) (from [32]).

Figure 7: Top: AOO fundus camera imaging of a GA case illustrating the similarities between punctuate hyperreflectivity (PHR) and the cone mosaic (CM). The dotted line represents the progression front. Note that some HRCs are superimposed with the PHR. Bottom, comparison of flood versus bright field scan AOO of the PHR and presumed CM at

941 the border of an atrophic lesion. While the CM is dim in bright field scan and/or blurred in
942 fundus camera AOO, within the atrophy areas there is a hyperreflective granular structure (i.e.
943 the PHR) of appearance and spacing similar to the CM.
944 **Figure 8**. Histology of BlamD (arrowheads) in an atrophic area of a GA eye (from
945 *projectmacula.cis.uab.edu).* Note the spiky surface of the BlamD.
946 **Figure 9**: Comparison of fundus camera versus scanning AOO of HRCs. Fundus camera
947 AOO shows HRCs as dark spots, while with scanning AOO they are less contrasted (arrows).
948 **Figure 10:** Example of migration patterns of HRCs (arrows) seen by fundus camera AOO.
949 Top row: migration in parallel to the progression of atrophy (b, c, and d: zoom of the area
950 shown in a, showing the progression of atrophy over 6 months). Bottom row: linear
951 progression (g: recapitulation over 8 months).
952 **Figure 11**: Illustration of the migration of an HRC (solid arrowhead) ahead of atrophy
953 progression seen by fundus camera AOO. The hollow arrowhead recapitulates the successive
954 position of the HRC s in previous images.
955 **Figure 12**: Comparison of histology and AOO images of a case of dry AMD. Presumptive
956 RPE cell types described by Zanzoterra et al.[19] are shown.
957 **Figure 13**: Outer retinal tubulations (ORT) seen with fundus camera AOO (A) and by bright
958 and dark field scanning AAO (B and C respectively). A: ORT in a case of dry AMD
959 (delineated by arrowheads). B and C, ORT in a case of retinal dystrophy. A long ORT (black
960 arrows) and several smaller ORT (white arrows) are seen extending from the less abnormal
961 region of retina into the atrophic region. Inserted are magnifications of the bright and dark
962 field, respectively, showing cones extending onto the ORT (Scale bars = 200 μm) (modified
963 from [56])

964 **Figure 14**. Illustration of the colocalization of short-wavelength autofluorescence (lipofuscin)
965 and melanin in a retinal flat-mount of a GA case. The upper row shows immunolabelling of
966 the actin cytoskeleton indicating confluence of RPE cells (modified from [37]).
967 **Figure 15**. AOO fundus camera imaging of a normal arteriovenous pair. In the
968 magnifications, arrowheads show the arterial and venous wall.
969 **Figure 16:** Details of parietal structures in an arteriole obtained by fundus camera AOO (left;
970 from author Serge Meimon) and with an offset aperture AOSLO (modified from [67]). Note
971 details of fine parietal structures, which may correspond to mural cells (black arrows).
972 **Figure 17**: Imaging of venous confluences showing the alignment of red blood cell columns.
973 Left, fundus camera AOO image. Three red blood cell columns (numerated 1 to 3) can be
974 followed in pre and post-confluence vessels. Center and right, scanning AOO bright and dark
975 motion contrast image (TBC), respectively. In the latter note the presence of at least three
976 distinct red cell columns (from[71]).
977 **Figure 18**: Mathematical relationship between the variations of vessel diameter on the
978 junction coefficient at an optimal bifurcation with initial values for the parent vessel (P) of
979 100µm and for daughter vessels (D_1 and D_2) of 79.37µm (which implies X=3). Each curve
980 represents the variations of X following the variation of the diameter of one vessel (P or D_1).
981 Overall, an increased X implies an increased downstream conductance which may be due to
982 upstream constriction or downstream dilation. For instance when P increases by 10µm, X will
983 increase to ~ 4.
984 **Figure 19**. Montage scanning AOO bright field image of the perifoveal capillaries using
985 motion contrast (from [108]) (scale bar, 250µm).
986 **Figure 20**: Fundus camera AOO images of venous nicking with (left) and without (center)
987 arteriovenous overlapping. Note in the central image the absence of detectable arteriovenous

contact. Right, focal arterial narrowing (FAN); zoom shows that the inner and outer limits of the wall remain parallel within the FAN.

Figure 21: Examples of fundus camera AAO imaging of advanced diabetic retinopathy showing from left to right microaneurysms, hard exudates and microhemorrhages.

Figure 22: Fundus camera AOO montage showing paravenous infiltrates (arrows) in a case of idiopathic vasculitis.

Figure 23: Evolution of a paravenous inflammatory infiltrate. A: fluorescein angiography; B: Fundus camera AOO showing in the boxed area a perivenous infiltrate. C to D: follow-up on the perivenous infiltrate. Note that the resolution of the infiltrate seems to coincide with restauration of venous caliber and also with the resolution of the displacement of axonal fibers (arrowheads).

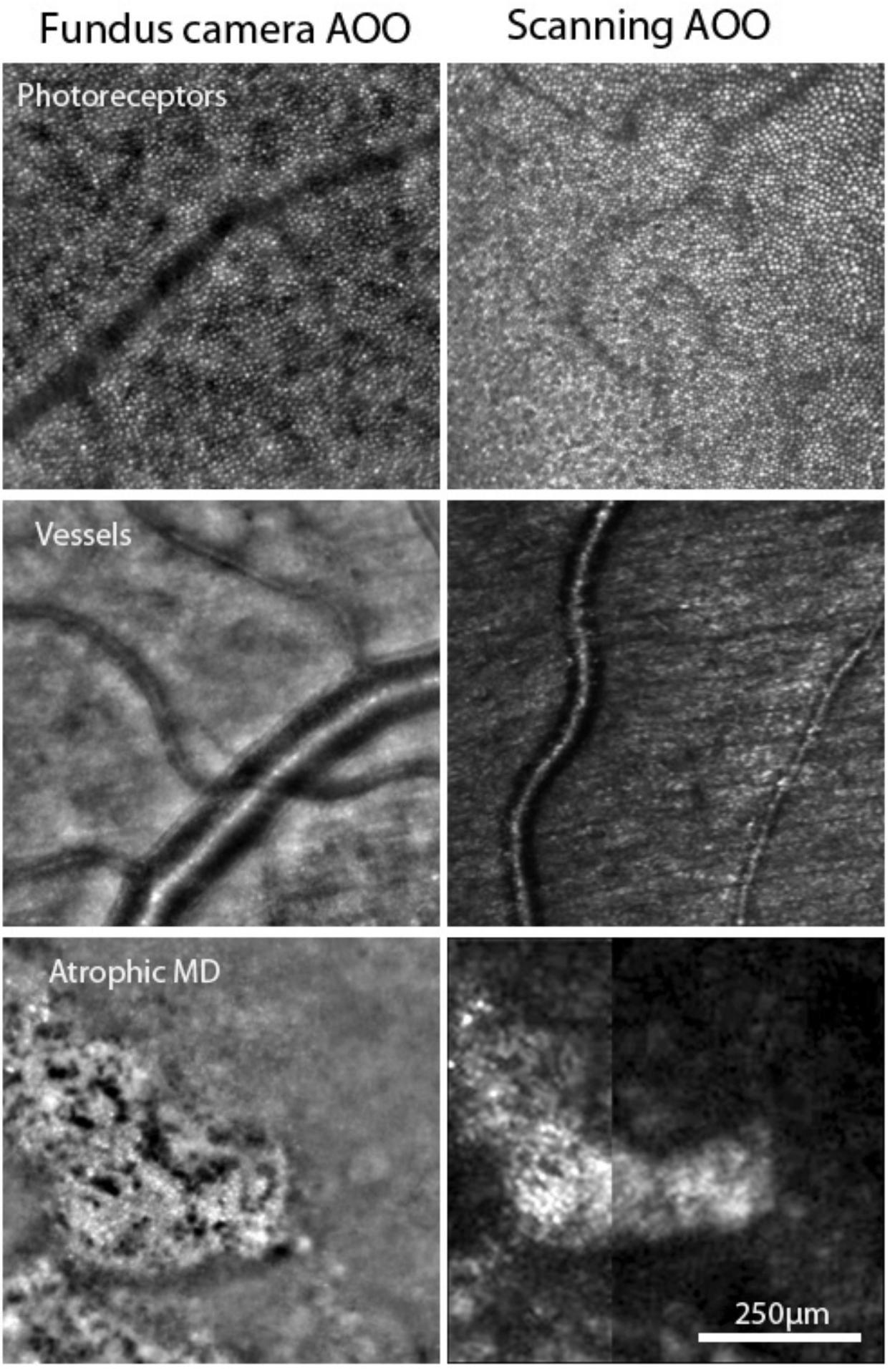
Fundus camera AOO
Scanning AOO
Photoreceptors
Vessels
Atrophic MD
250µm

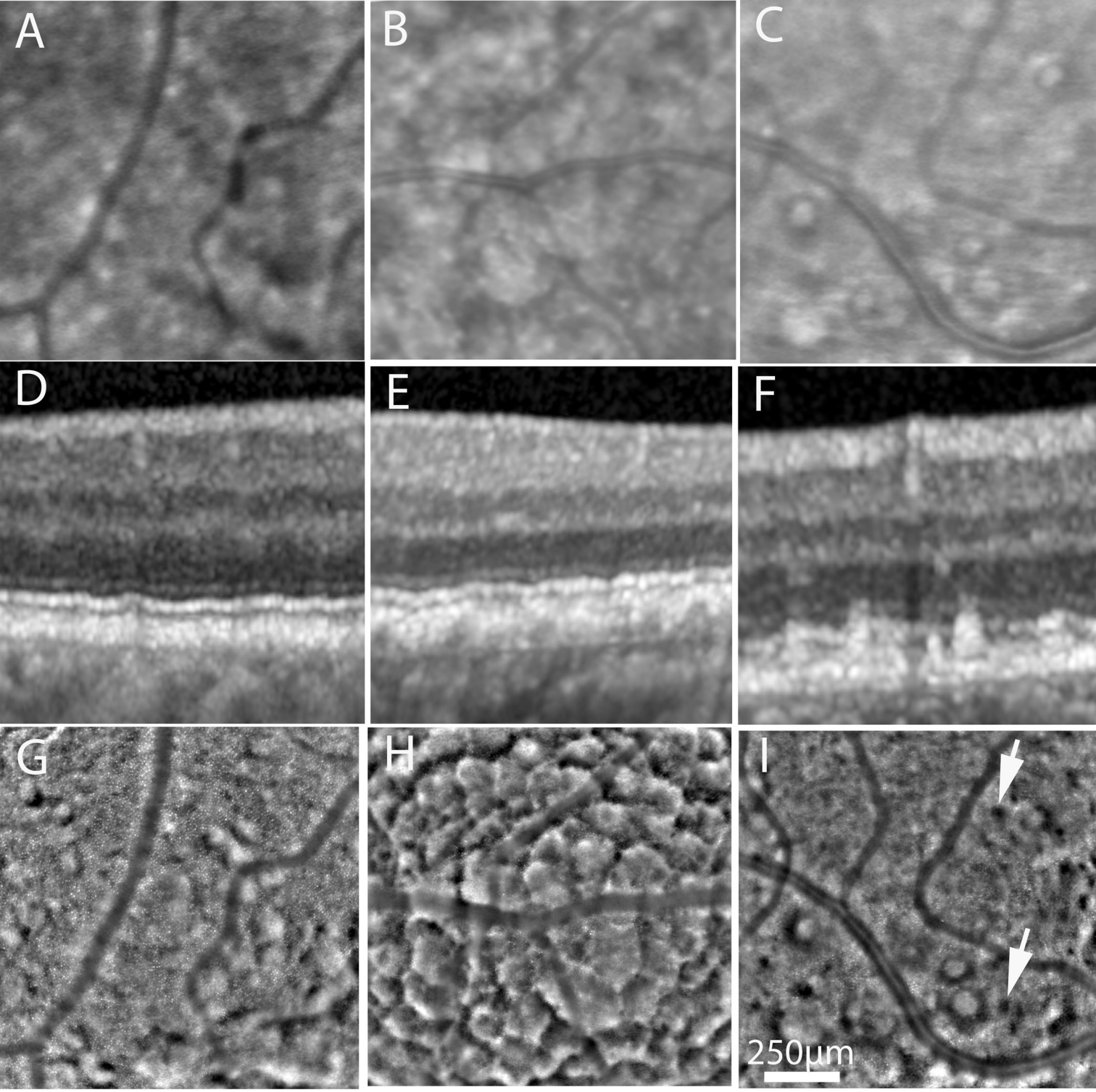
A
B
C
D
E
F
G
H
I
250µm

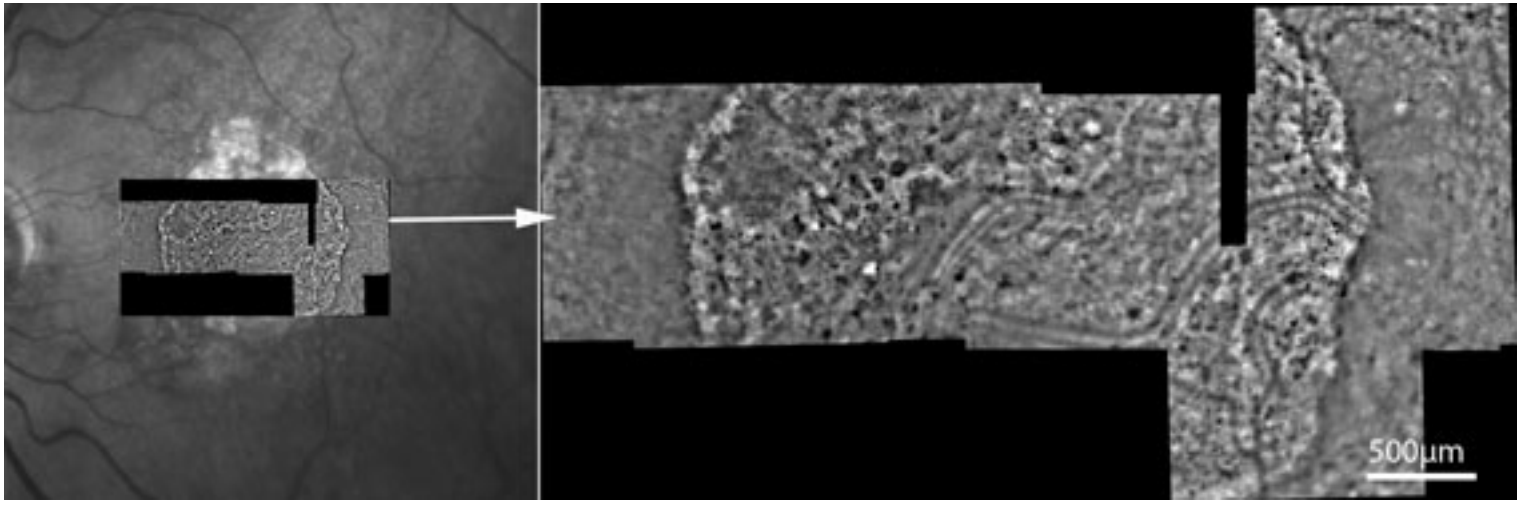
500µm

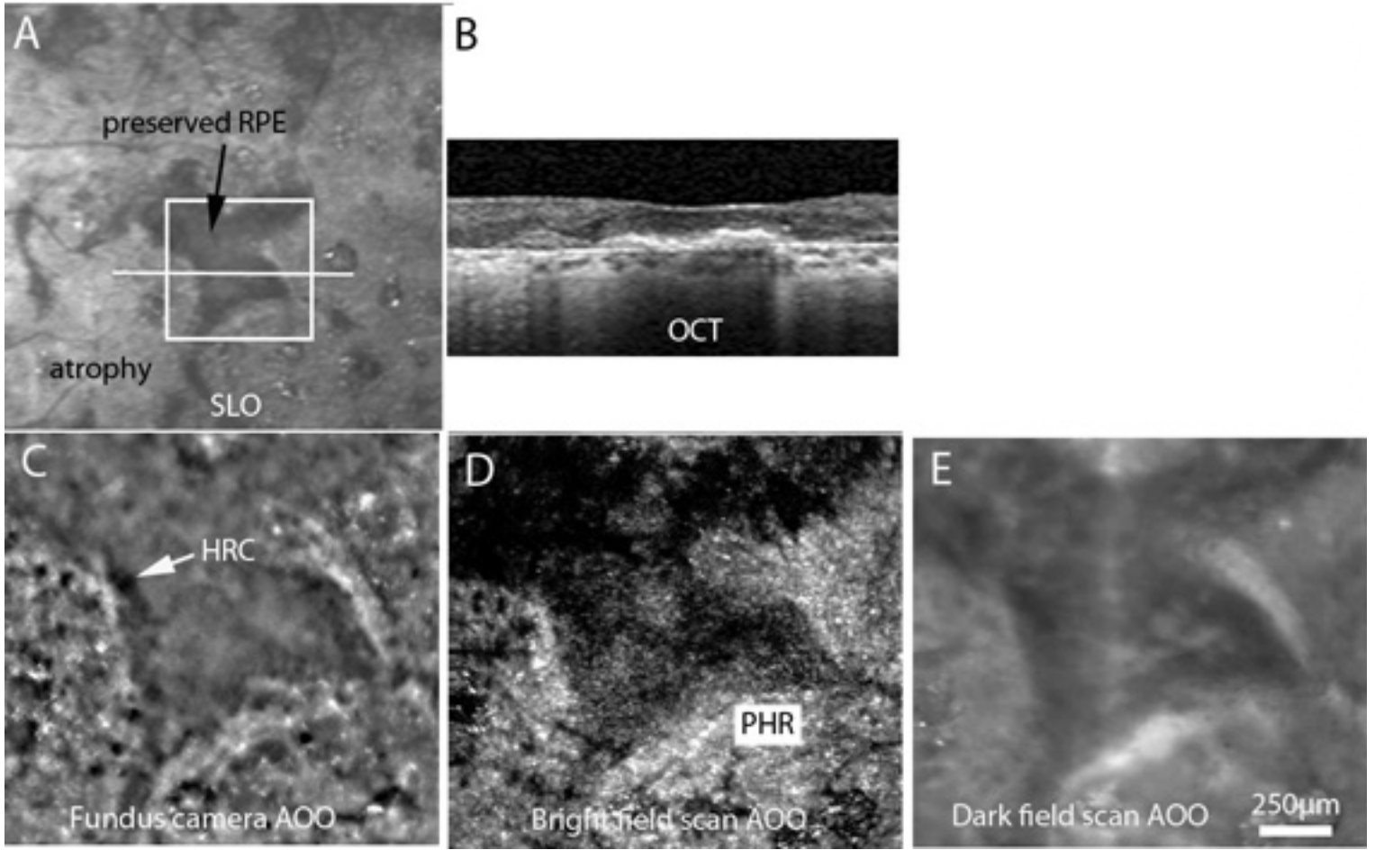
A
preserved RPE
atrophy
SLO
B
OCT
C
HRC
Fundus camera AOO
D
PHR
Bright field scan AOO
E
Dark field scan AOO
250µm

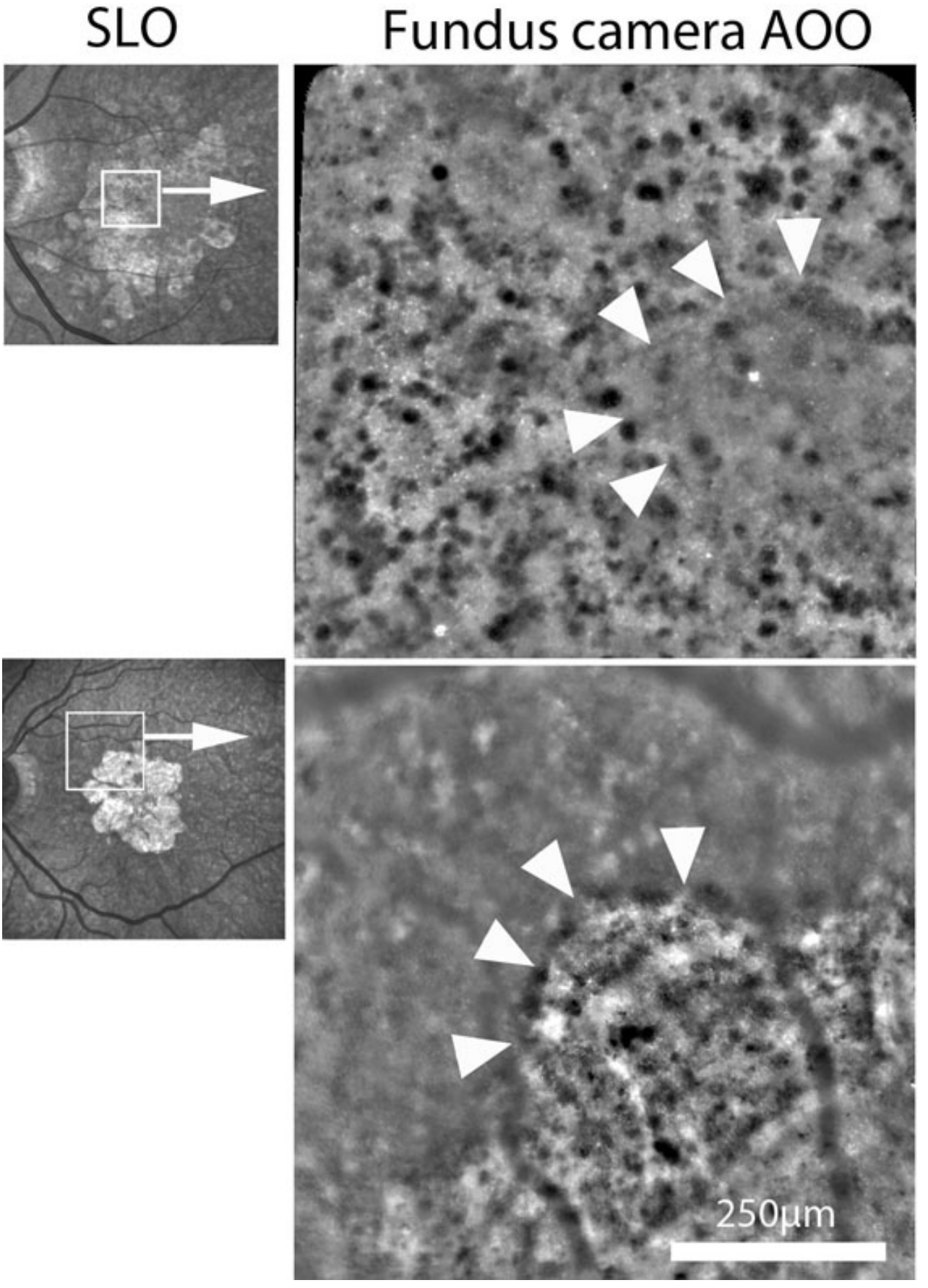
SLO
Fundus camera AOO
250µm

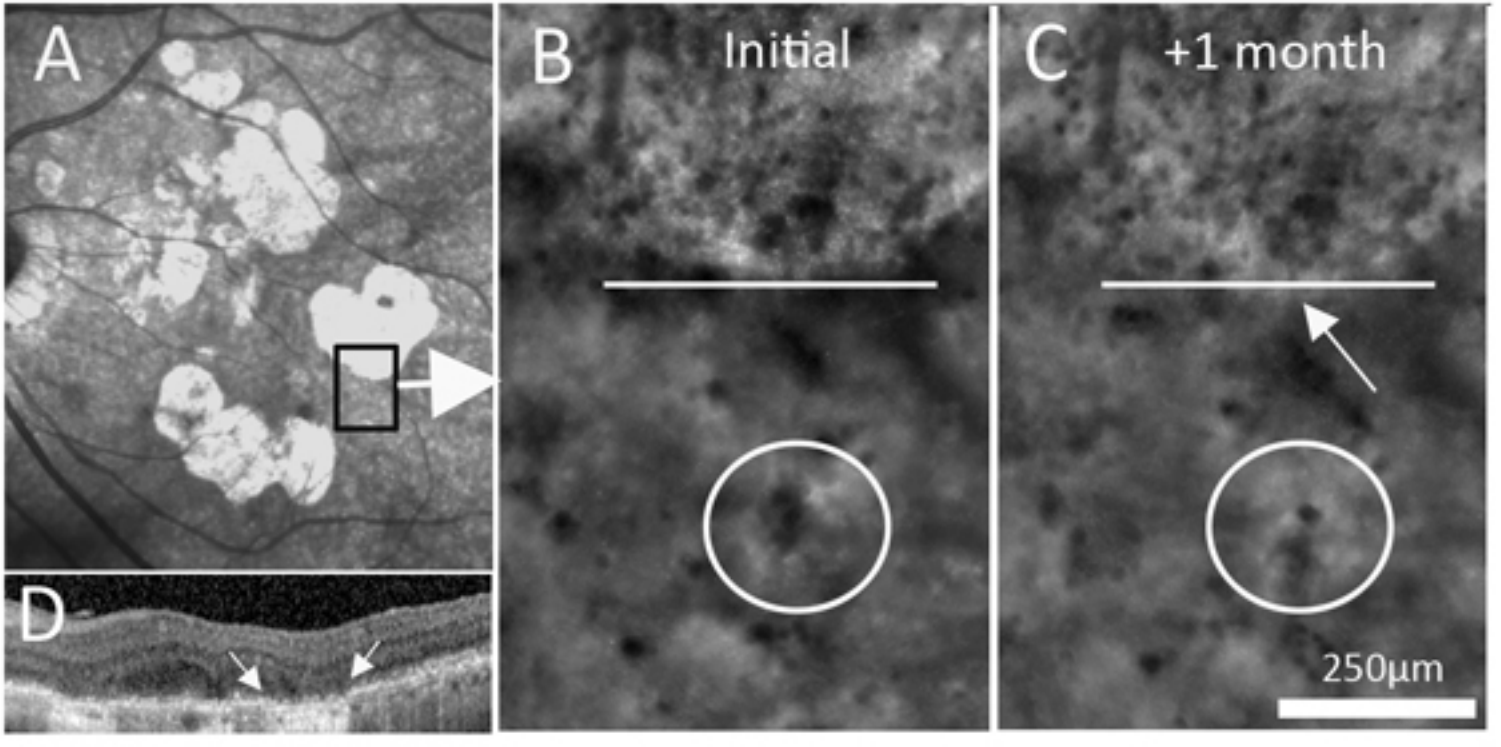
A
B
Initial
C
+1 month
D
250µm

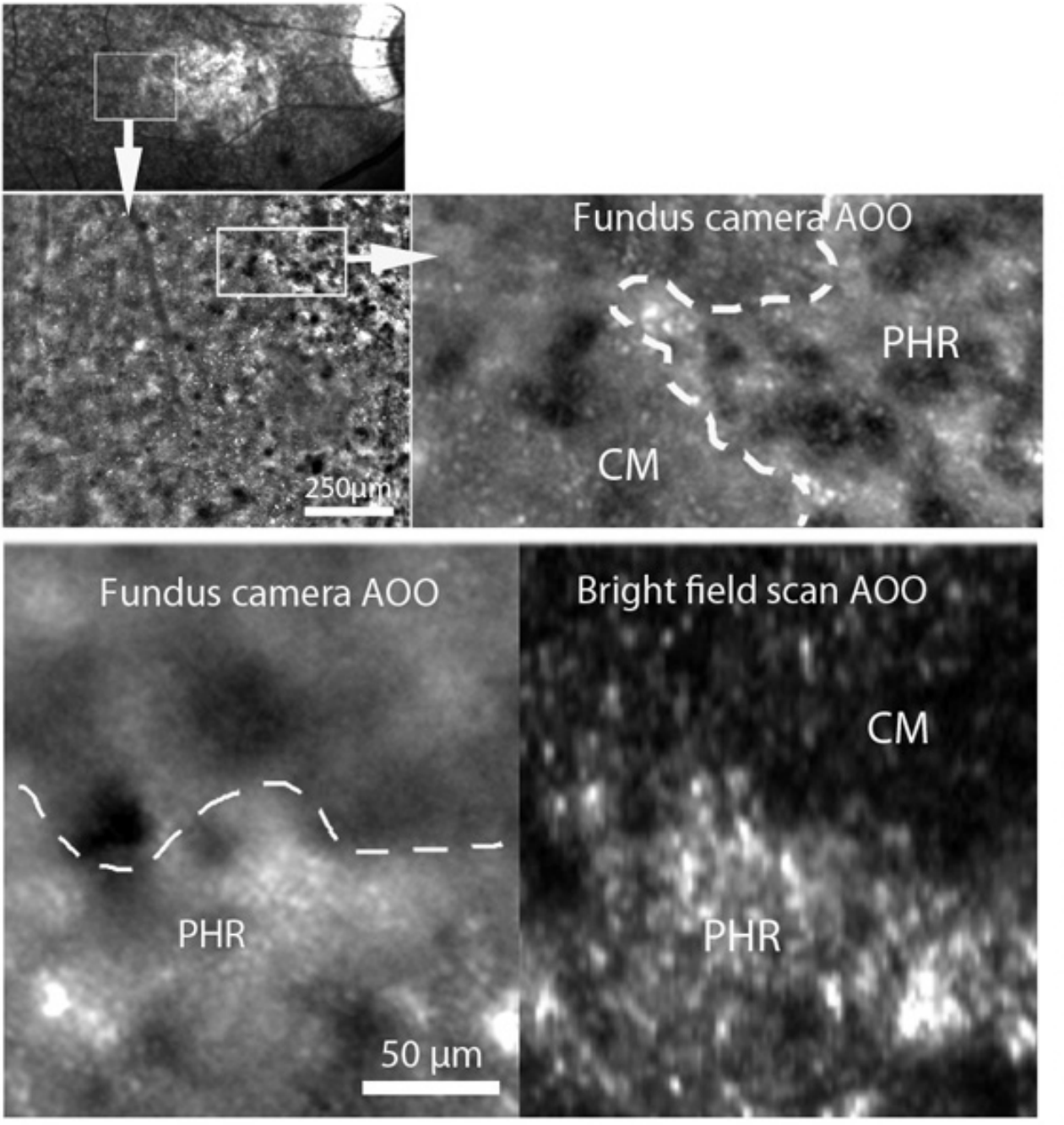
Fundus camera AOO
PHR
CM
250µm
Fundus camera AOO
Bright field scan AOO
CM
PHR
PHR
50 µm

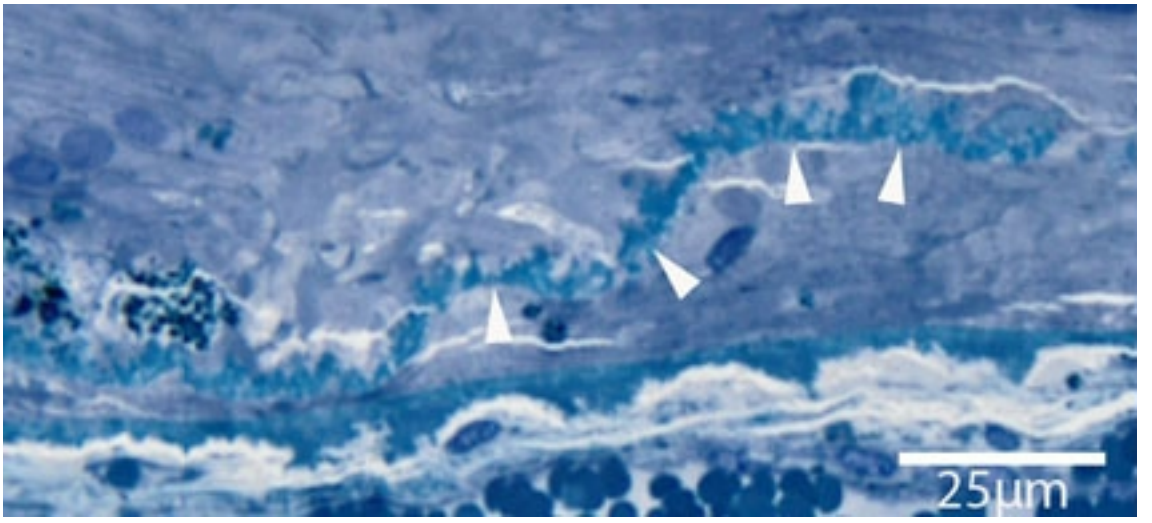
25μm

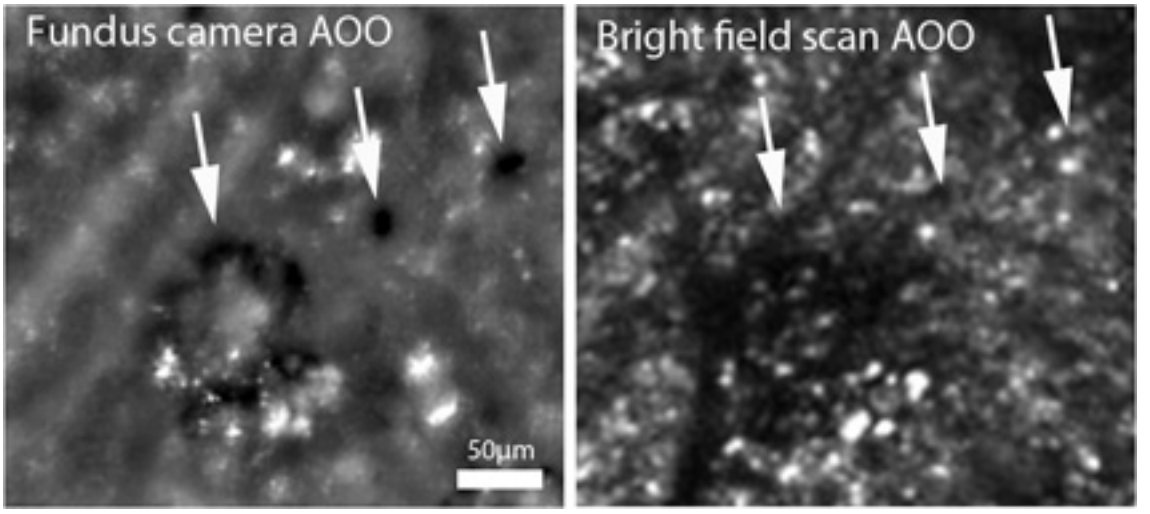
Fundus camera AOO
50µm
Bright field scan AOO

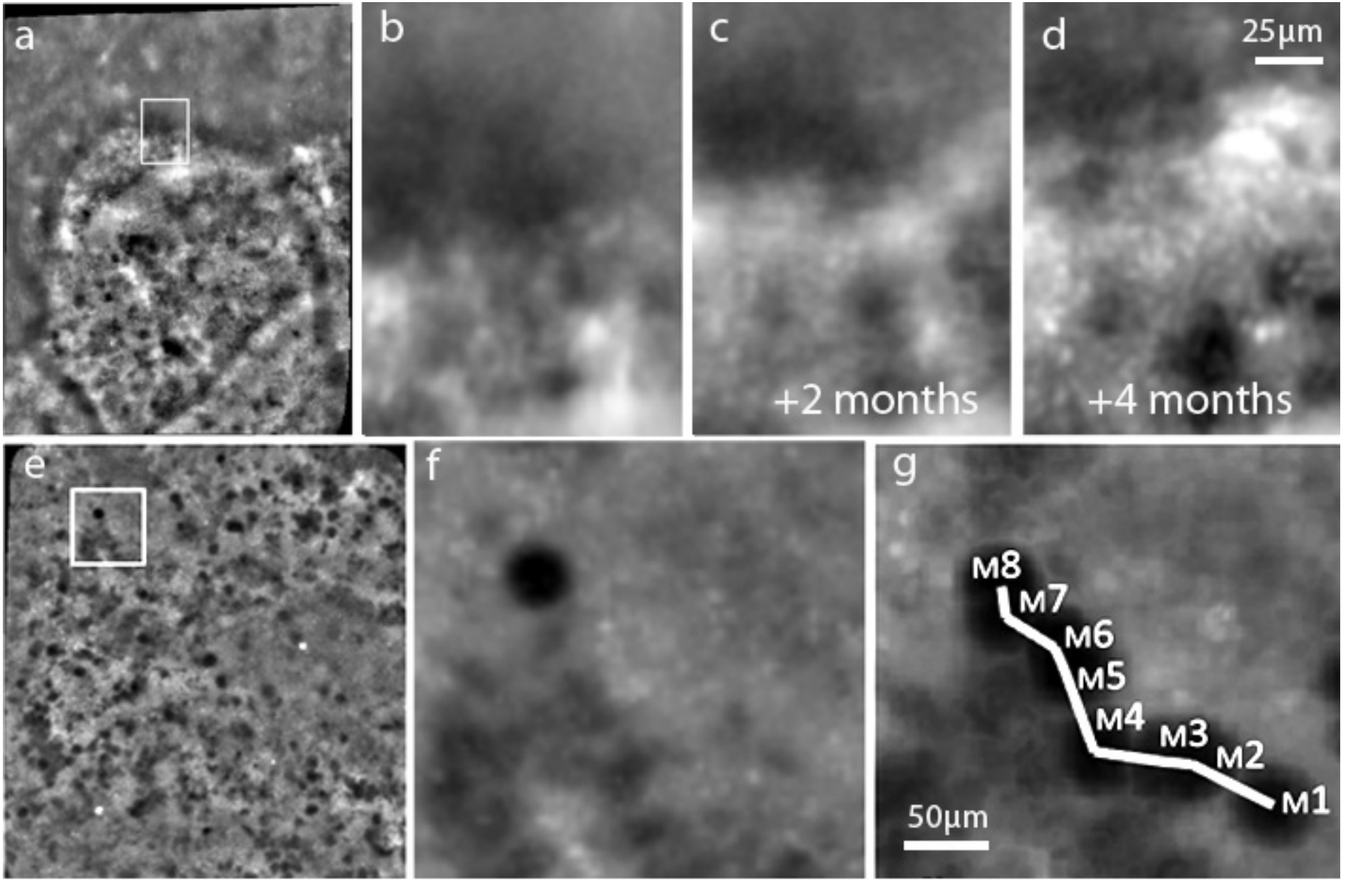
a
b
c
+2 months
d
25µm
+4 months
e
f
g
M8
M7
M6
M5
M4
M3
M2
M1
50µm

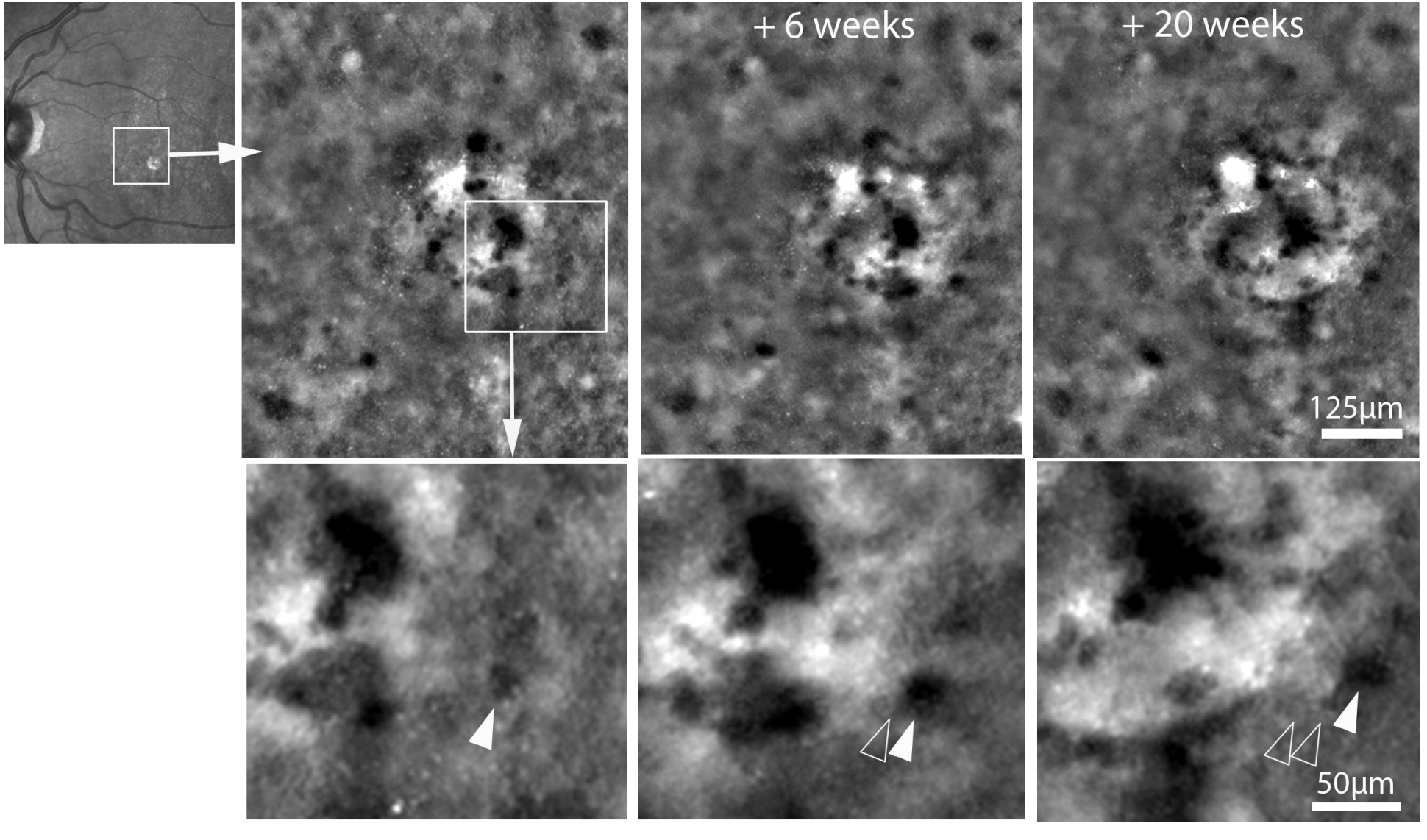
+ 6 weeks
+ 20 weeks
125µm
50µm

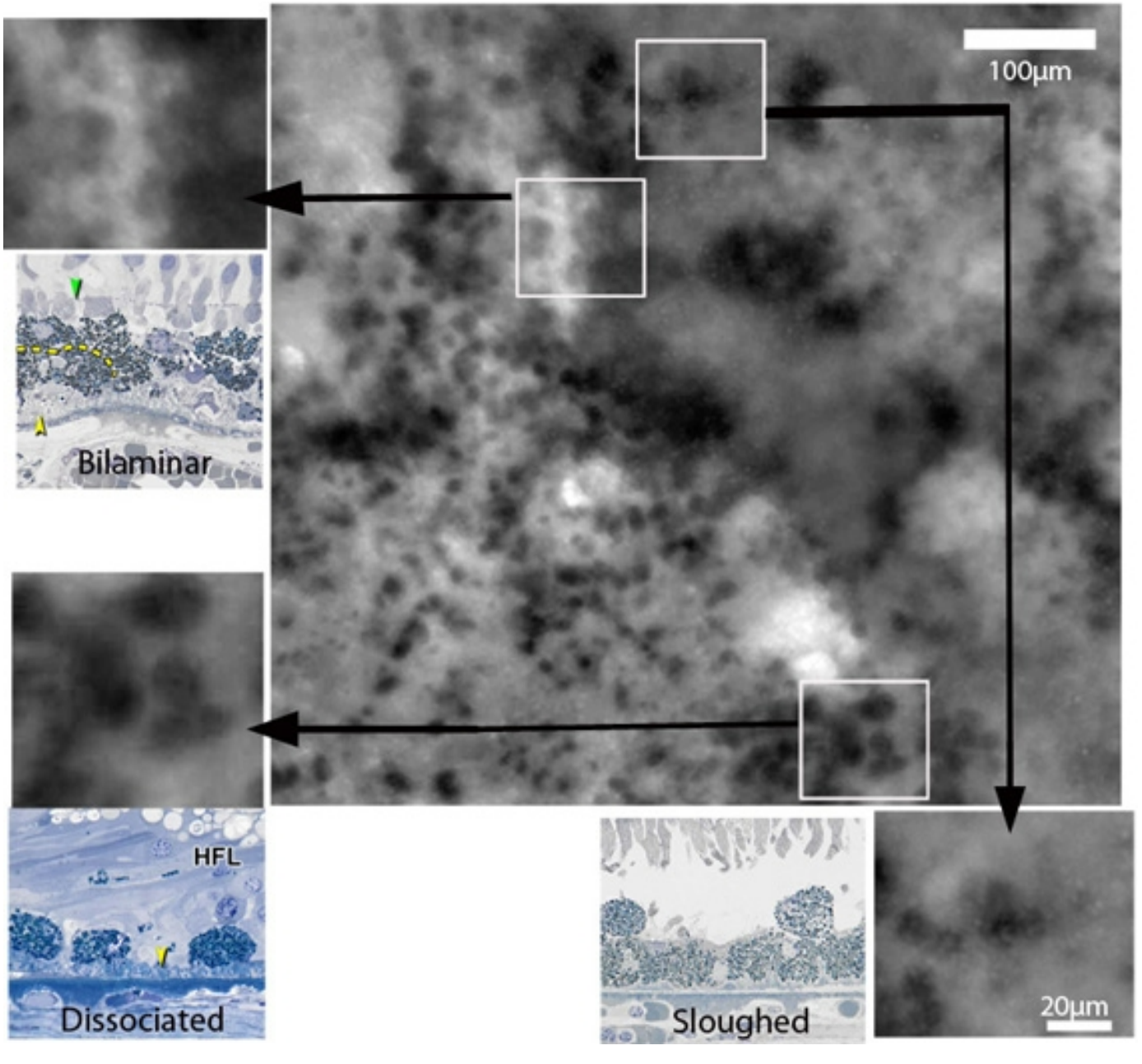
100µm
Bilaminar
HFL
Dissociated
Sloughed
20µm

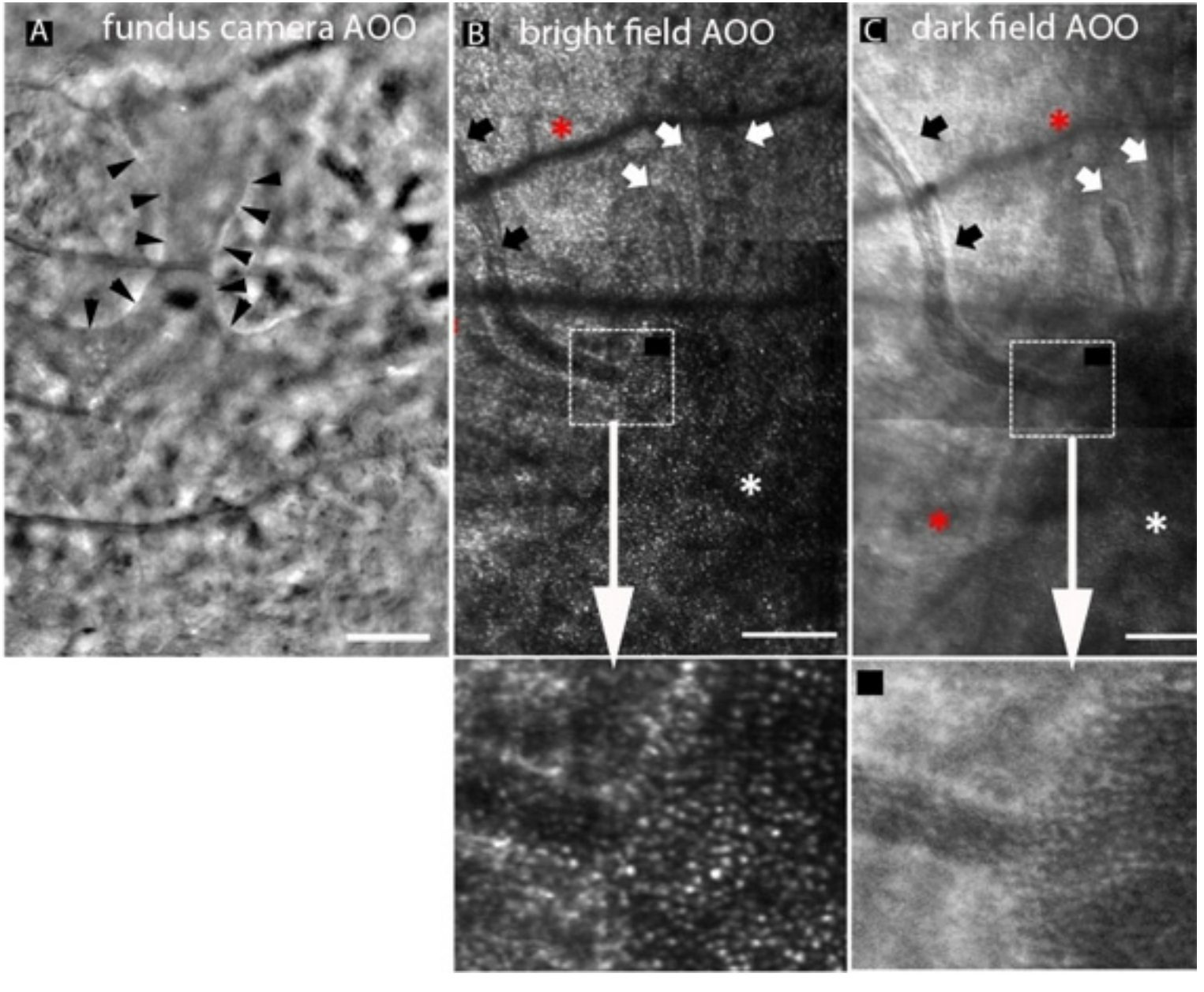
A
fundus camera AOO
B
bright field AOO
C
dark field AOO

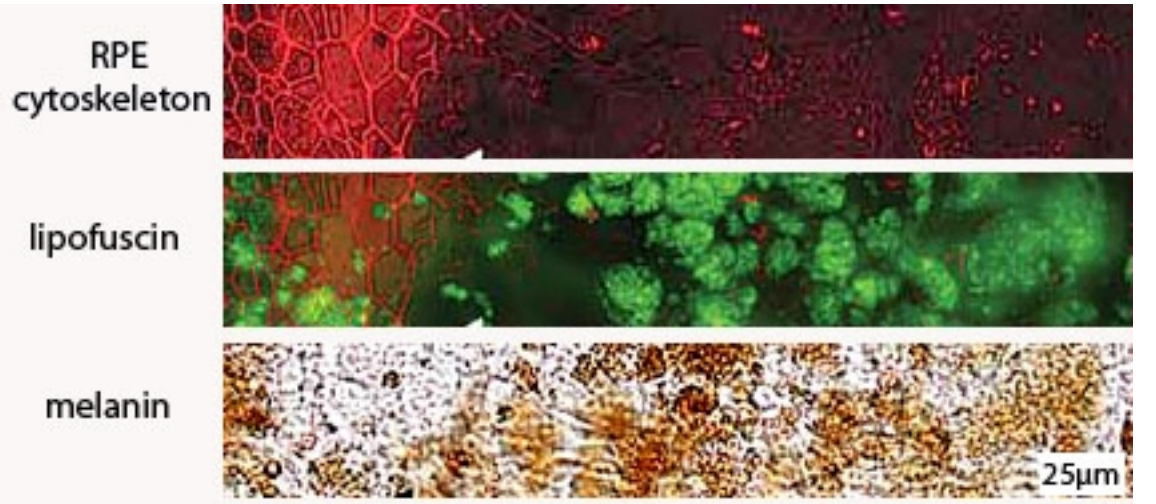
RPE
cytoskeleton
lipofuscin
melanin
25µm

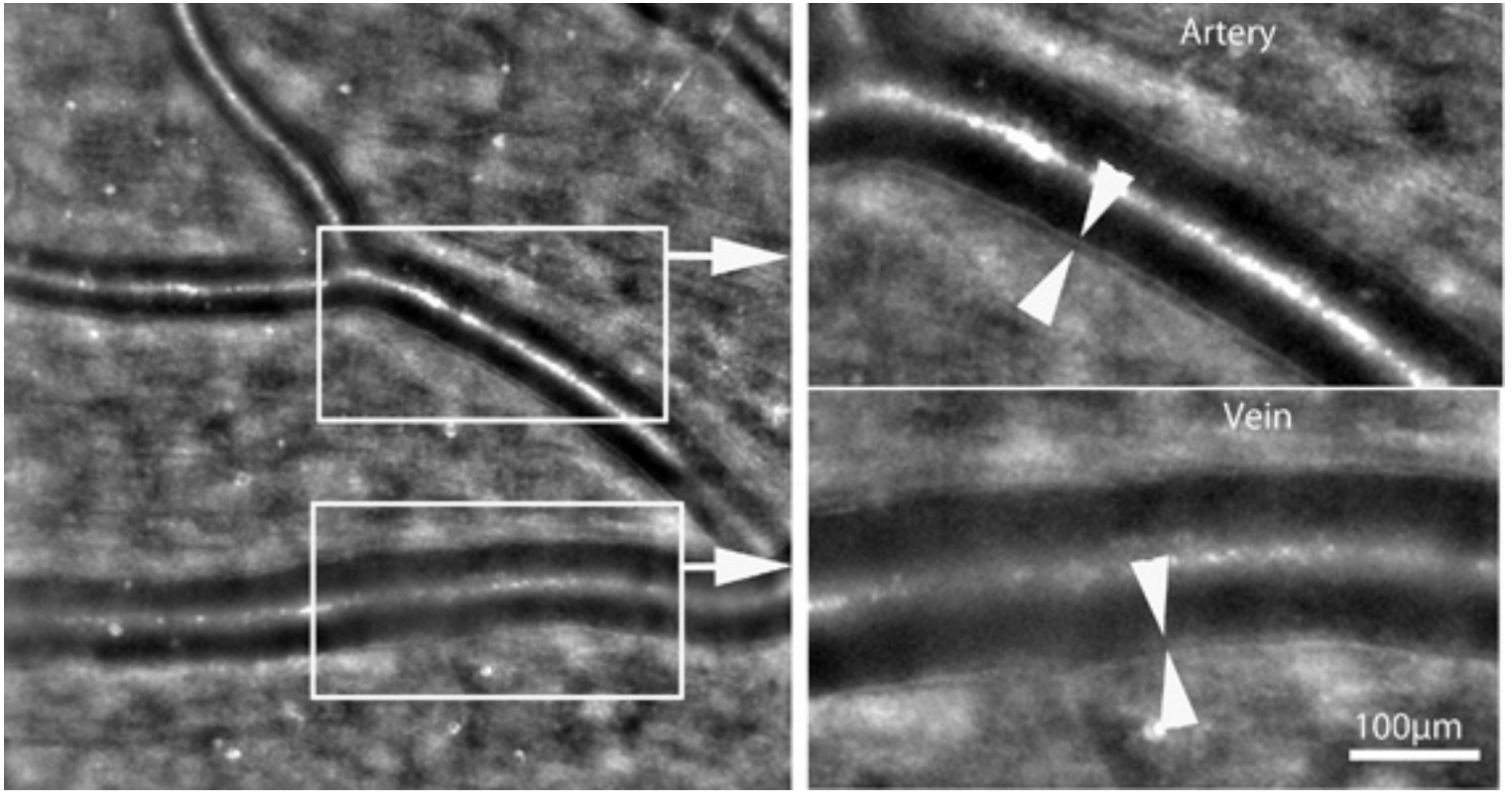
Artery
Vein
100µm

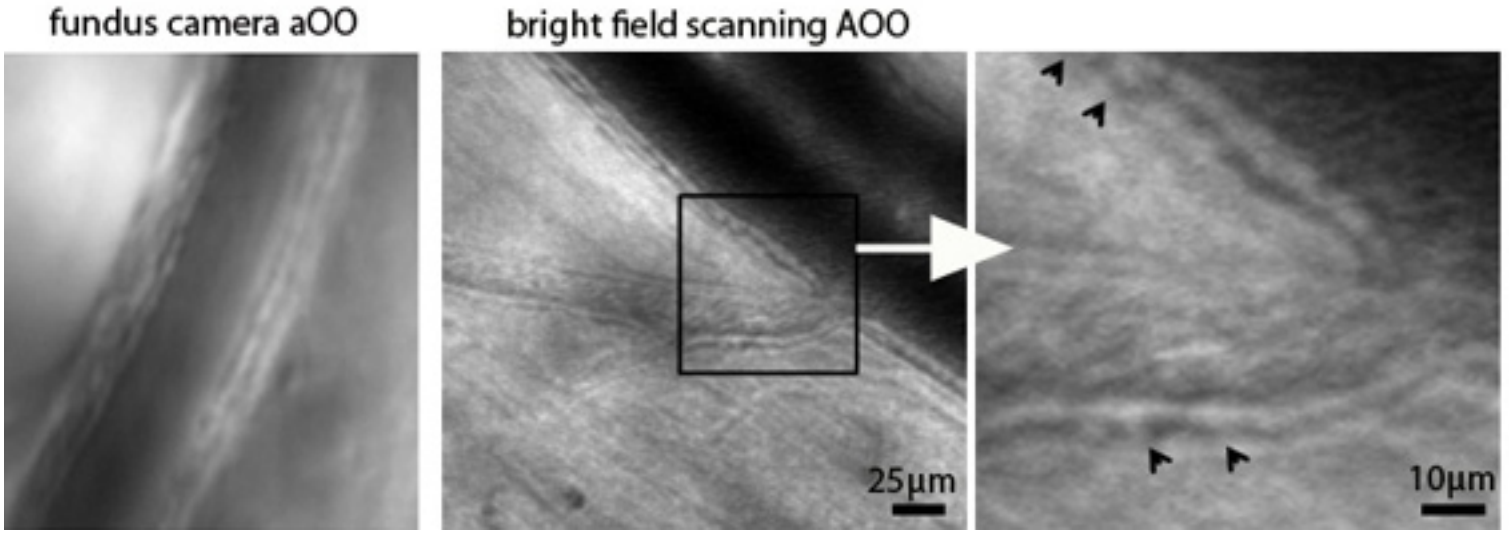
fundus camera aOO
bright field scanning AOO
25µm
10µm

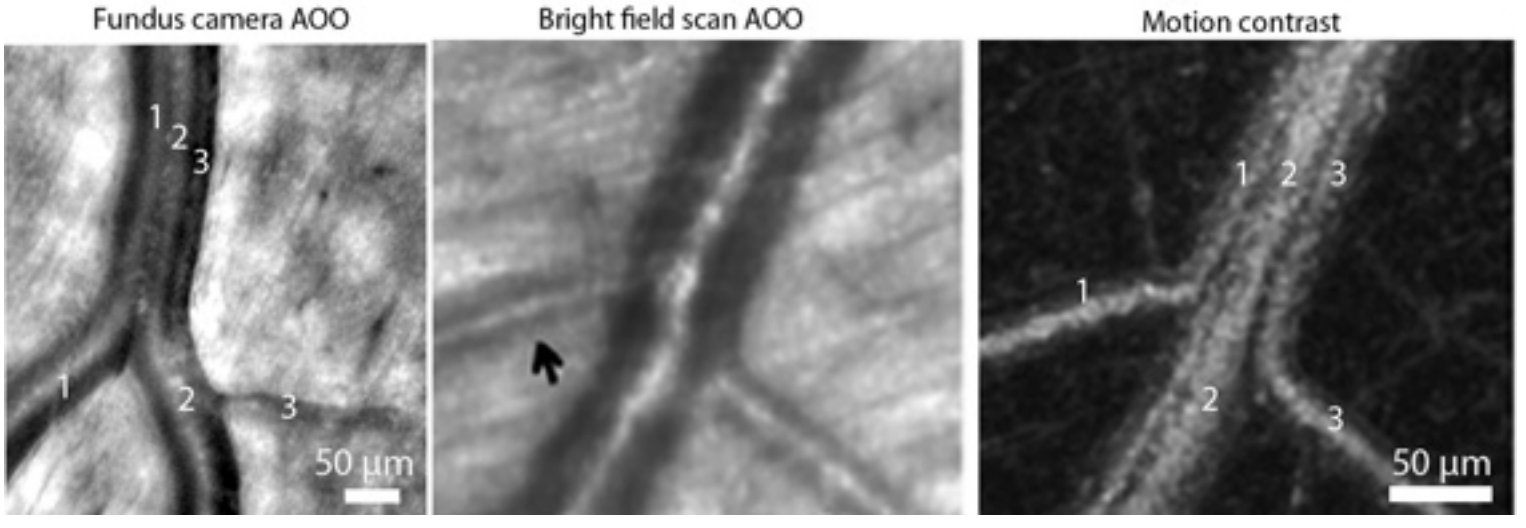
Fundus camera AOO
Bright field scan AOO
Motion contrast
1
2
3
1
2
3
50 µm
1
2
3
1
2
3
50 µm

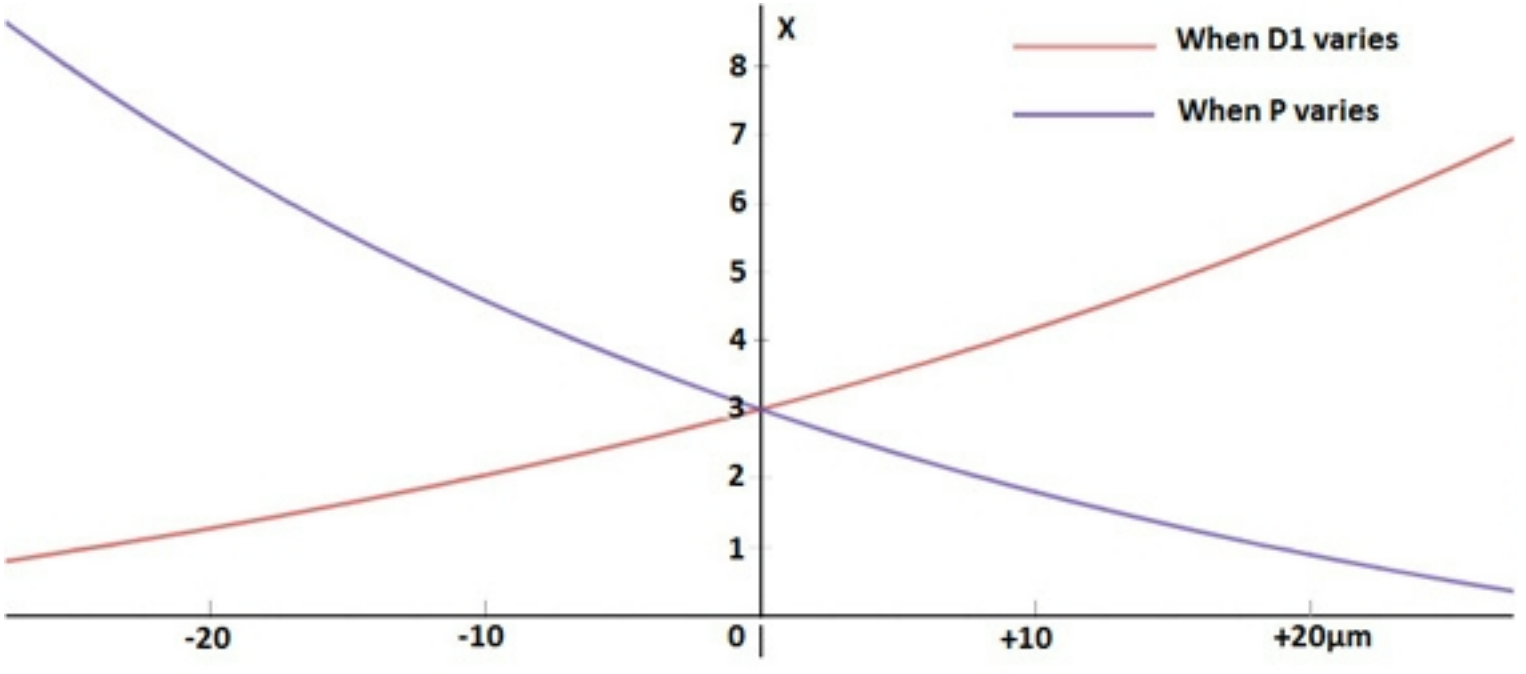
X
When D1 varies
When P varies
8
7
6
5
4
3
2
1
-20
-10
0
+10
+20µm

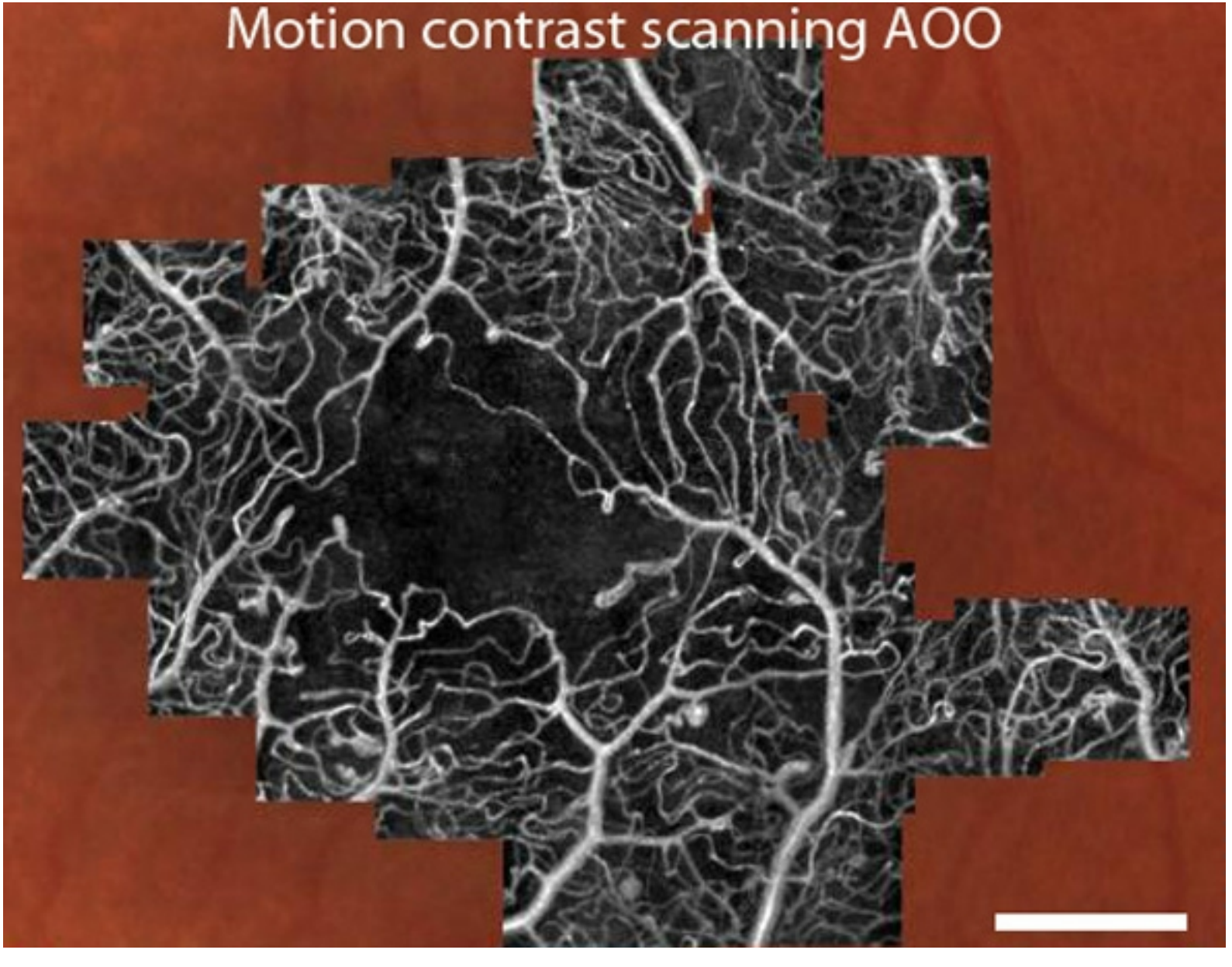
Motion contrast scanning AOO

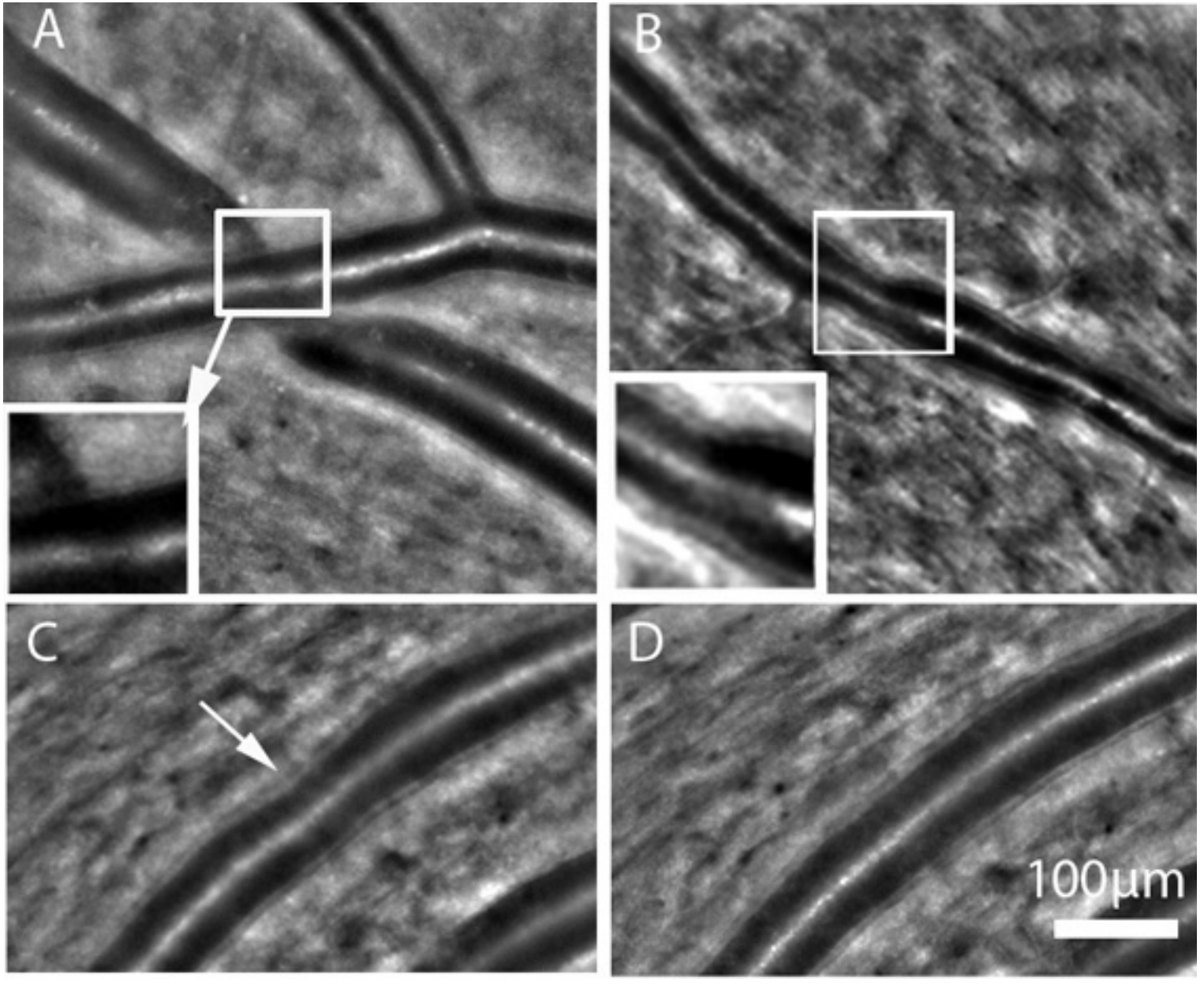
A
B
C
D
100µm

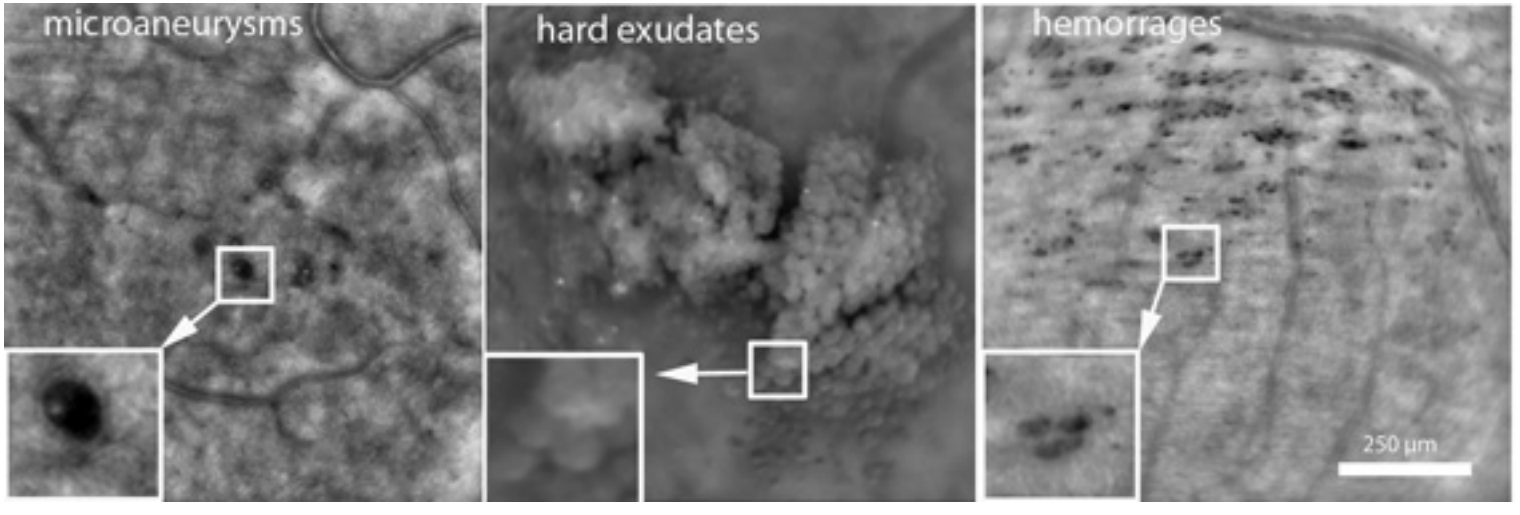
microaneurysms
hard exudates
hemorrages
250 µm

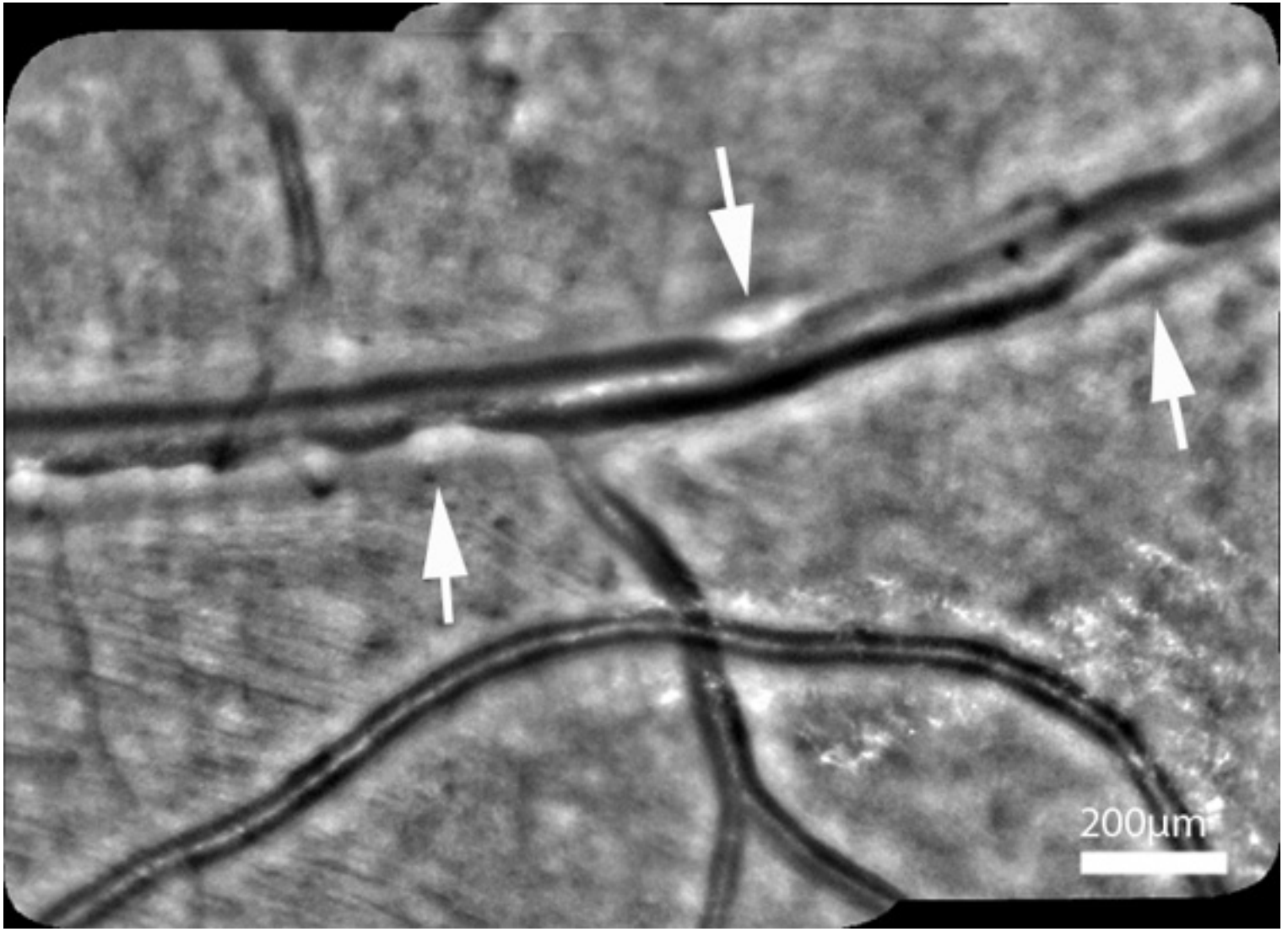
200µm

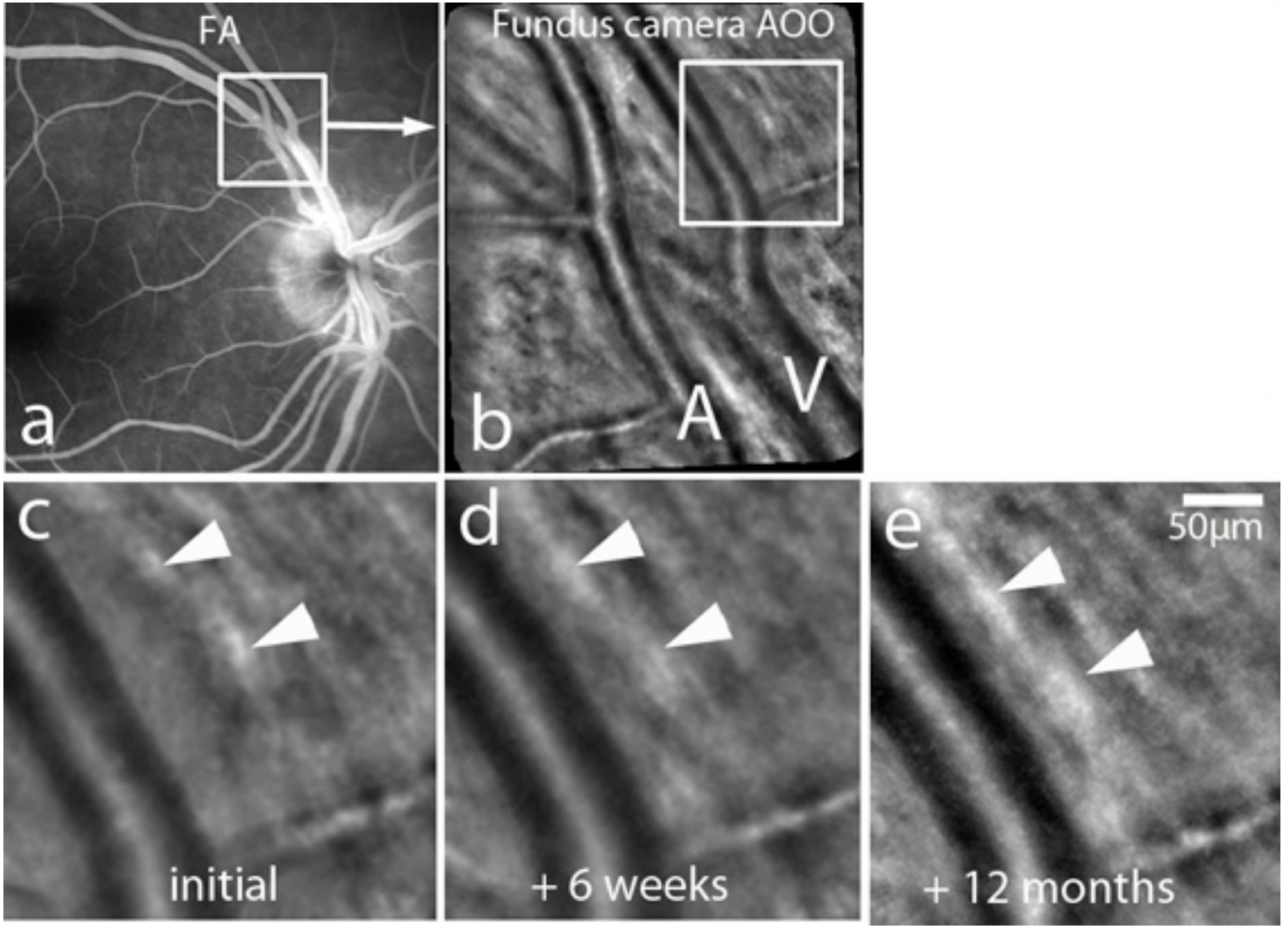
FA
Fundus camera AOO
a
b
A
V
c
d
e
50µm
initial
+ 6 weeks
+ 12 months